

# Three decades of deep water mass investigation in the Weddell Sea (1984–2014): temporal variability and changes

Rodrigo Kerr<sup>1,2,\*</sup>, Tiago S. Dotto<sup>1,2,\*a</sup>, Mauricio M. Mata<sup>1,2</sup>, and Hartmut H. Hellmer<sup>3</sup>

<sup>1</sup>Laboratório de Estudos dos Oceanos e Clima, Instituto de Oceanografia, Universidade Federal do Rio Grande – FURG, Rio Grande, RS, 96203-900, Brazil.

<sup>2</sup>Grupo de Estudos do Oceano Austral e Gelo Marinho, Instituto Nacional de Ciência e Tecnologia da Criosfera (INCT-CRIOSFERA), Rio Grande, 96203-900, RS, Brazil.

<sup>3</sup>Stiftung Alfred-Wegener-Institut für Polar- und Meeresforschung in der Helmholtz-Gemeinschaft, Bussestraße 24, 27570 Bremerhaven, Germany.

\*These authors contributed equally to this work.

<sup>a</sup>Now at: Ocean and Earth Science, University of Southampton, National Oceanography Centre, Southampton, UK.

\*Corresponding author:

Address: Instituto de Oceanografia, Universidade Federal do Rio Grande – FURG, Avenida Itália km 8 s/n°, Campus Carreiros, Rio Grande – RS, Brazil, 96203–900

E-mail: [rodrigokerr@furg.br](mailto:rodrigokerr@furg.br); [tiagosdotto@gmail.com](mailto:tiagosdotto@gmail.com)

Phone number: +55 53 3233-6858

Running title: Weddell deep waters variability

## 1 **Highlights**

- 2 • Shifts in Weddell Sea Bottom Water (WSBW) properties towards less dense
- 3 varieties likely equate to less WSBW being produced over time.
- 4 • The decline of WSBW volume ceased around 2005 and likely recovering after
- 5 that.
- 6 • Dense Shelf Waters drive and modulate the recent WSBW variability.
- 7 • WSBW is composed by 71% of Warm Deep Water and 29% of Dense Shelf
- 8 Waters.

9

## 10 **Abstract**

11 The role of Antarctic Bottom Water (AABW) in changing the ocean circulation  
12 and controlling climate variability is widely known. However, a comprehensive  
13 understanding of the relative contribution and variability of Antarctic regional deep water  
14 mass varieties that form AABW is still lacking. Using a high-quality dataset comprising  
15 three decades of observational shipboard surveys in the Weddell Sea (1984–2014), we  
16 updated the structure, composition and hydrographic properties variability of the Weddell  
17 Sea deep-layer, and quantified the contribution of the source waters composing Weddell  
18 Sea Bottom Water (WSBW) in its main formation zone. Shifts in WSBW hydrographic  
19 properties towards less dense varieties likely equate to less WSBW being produced over  
20 time. WSBW is primarily composed of  $71\pm 4\%$  of modified-Warm Deep Water (mWDW)  
21 and  $29\pm 4\%$  of Dense Shelf Waters, with the latter composed by ~two-thirds ( $19\pm 2\%$ ) of  
22 High Salinity Shelf Water and ~one-third ( $10\pm 6\%$ ) of Ice Shelf Water. Further, we show  
23 evidence that WSBW variability in the eastern Weddell Sea is driven by changes in the  
24 inflow of Dense Shelf Waters and bottom water from the Indian Sector of the Southern  
25 Ocean. This was observed through the rise of the WSBW contribution to the total mixture  
26 after 2005, following a twenty-year period (1984–2004) of decreasing contribution.

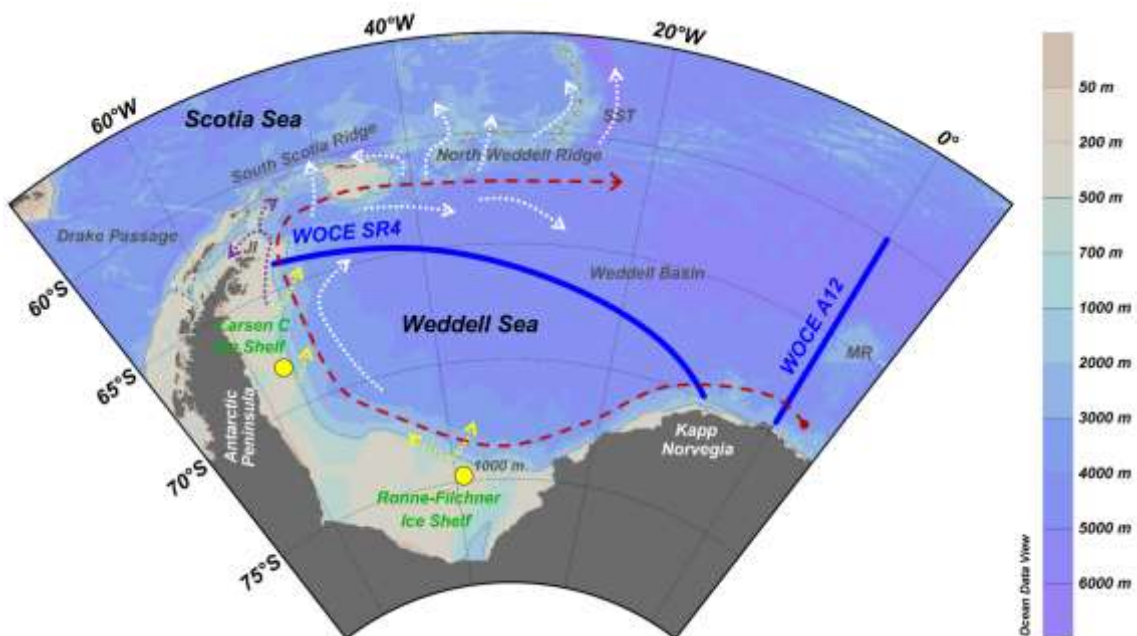
27 **Key words:** Deep Ocean, Antarctic Bottom Water, Dense Shelf Water, Southern Ocean.

## 28 **1. Introduction**

29           Several recent studies have debated about the causes and effects of Antarctic  
30 Bottom Water (AABW) variability and changes both in its source area and throughout  
31 the global ocean (e.g., Schmidtko et al. 2014; Azaneu et al., 2013; Purkey and Johnson,  
32 2010, 2012, 2013). AABW is one of the major water mass of the lower limb of the global  
33 overturning circulation (e.g. Talley, 2013) and is composed of distinct regional dense  
34 water varieties sourced and/or modified around the Antarctic continent (e.g. Whitworth  
35 et al., 1998; Pardo et al., 2012). Its formation is driven by numerous coupled ocean-  
36 atmosphere-cryosphere processes taking place in the Southern Ocean (e.g., ocean-  
37 atmosphere heat fluxes, sea ice formation and melting, ocean-ice-shelf interaction, water  
38 mass mixing, ocean frontal instabilities, etc.). Briefly, those coupled processes increase  
39 the water mass density in the resulting mixture, which eventually leads to a dense plume  
40 overflow down the continental slope towards the deep ocean (Orsi et al., 1999; 2001;  
41 Ivanov et al., 2004; Nicholls et al., 2009).

42           Two distinct AABW formation processes have been previously described in the  
43 Weddell Sea (Fig. 1), the source region of the main AABW regional variety exported to  
44 the global ocean (e.g. Orsi et al., 2002; Kerr et al., 2012a; van Seville et al., 2013; Ferreira  
45 and Kerr, 2017). The first one was proposed by Foster and Carmack (1976a) after  
46 intensive studies in the Weddell Sea during the 1970s (e.g., Carmack, 1974; Carmack and  
47 Foster, 1975a, 1975b; Foster and Carmack, 1976b). It assumes that the mixing of dense  
48 High Salinity Shelf Water (HSSW) and modified-Warm Deep Water (mWDW; a mixture  
49 of Winter Water (WW) and Warm Deep Water (WDW)) at the continental shelf-break in  
50 the southern Weddell Sea forms the densest AABW regional variety: Weddell Sea  
51 Bottom Water (WSBW). As the dense WSBW follows the continental slope, it remixes  
52 with WDW resulting in the less dense variety of AABW in the Weddell Sea: Weddell Sea

53 Deep Water (WSDW). Recently, van Caspel et al. (2016) showed that the Larsen Ice  
 54 Shelf region also plays a key role modulating the hydrographic properties and,  
 55 consequently, the formation process of AABW varieties in the northwestern Weddell Sea  
 56 (Gordon et al., 1993). The second process was introduced by Foldvik et al. (1985) and  
 57 involves the mixture of WDW/mWDW and Ice Shelf Water (ISW)—a water mass with  
 58 temperatures below surface freezing derived from the interaction of HSSW within the  
 59 base of the ice-shelves in the southern Weddell Sea (Nicholls et al., 2001, 2004).



60

61 **Figure 1.** The study area in the Weddell Sea showing the location of the hydrographic sections (solid blue  
 62 lines) across the Weddell Gyre (schematically indicated by the dashed red arrow) along the Greenwich  
 63 Meridian (southern part of WOCE A12 repeat line) and across the Weddell Sea (WOCE SR4 repeat line)  
 64 between Kapp Norvegia and Joinville Island (JI). The yellow dots mark the primary areas of AABW  
 65 varieties formation, while the yellow dotted arrows schematically show sinking water masses along the  
 66 continental slope. The dotted purple arrows indicate Dense Shelf Water living the northwestern Weddell  
 67 Sea. The dotted white arrows depict deep and bottom water circulation and water masses exporting the  
 68 Weddell Basin. This figure was sketched according to the studies of Gordon et al. (2001), von Gyldenfeldt  
 69 et al. (2002), Naveira Garabato et al. (2002), Fahrbach et al. (2011), and Ferreira and Kerr (2017). See  
 70 Table 1 for the sections occupation periods between 1984 and 2014. The bathymetry (m) is represented as  
 71 a color scale bar at the right. MR = Maud Rise; SST = South Sandwich Trench. Bathymetry line of 1000 m  
 72 is represented by the thin black line. (For interpretation of the references to color in this figure legend, the  
 73 reader is referred to the web version of this article.)

74

75 Whitworth et al. (1998), through a detailed study of all Antarctic margins,  
 76 proposed that WSBW can be formed by mixing of mWDW with HSSW or ISW

77 depending if the east or west side of the basin considered, i.e., combining the AABW  
78 formation processes proposed by Foster and Carmack (1976a) and Foldvik et al. (1985).  
79 A detailed review of ice-ocean processes on the continental shelf of the southern Weddell  
80 Sea was further compiled by Nicholls et al. (2009), whereas Heywood et al. (2014)  
81 summarized the processes at the Antarctic continental shelf-break that are important for  
82 cross-slope exchanges of heat, freshwater, nutrients, and biota. In summary, despite the  
83 local ocean-, atmosphere- and cryosphere-related processes involved in the formation of  
84 AABW varieties in the Weddell Sea sub-regions, WSDW and WSBW in the deep  
85 Weddell Basin can be considered as a mixture of WW (i.e. a remnant of the deep winter  
86 mixed layer), WDW, HSSW and ISW. The first two water masses mix and are modified  
87 through the dynamic processes occurring in the Weddell Gyre regime (often referred to  
88 as mWDW), while the AABW shelf-components are regionally confined and modified  
89 through the coastal, air-sea and ice-land-sea processes occurring in the continental shelf  
90 regime.

91       Much less often, deep ocean convection in open ocean polynyas can directly form  
92 and modulate AABW varieties in the Southern Ocean (Gordon, 1978; Gordon, 2014).  
93 Although the recent appearance of this phenomenon in 2016 and 2017, this has not been  
94 observed with the dimensions and persistence of the Weddell Polynya since the events  
95 occurred in the 1970s (Comiso and Gordon, 1987; Gordon et al., 2007). This process,  
96 although more related to coastal polynyas, may occur in other important AABW  
97 formation regions outside the Weddell Sea as well (Ohshima et al., 2013; Kitade et al.,  
98 2014). It is also important to consider that AABW varieties sourced in the Weddell Sea  
99 and present in the easternmost part of the Weddell Basin are strongly influenced by deep  
100 and bottom waters which originated to the East of the Weddell Sea (Meredith et al., 1999;  
101 2000). This AABW variety enters the Weddell Gyre from the Indian Sector of the

102 Southern Ocean, allowing further ventilation and densification of Weddell Sea AABW  
103 varieties within the gyre (Jullion et al., 2014).

104 AABW has a global and climate importance because it ventilates and renews the  
105 properties of the near-bottom layer of the global ocean (Schröder et al., 2002; Jacobs,  
106 2004; Ferreira and Kerr, 2017). Considering the Weddell Sea regional AABW varieties,  
107 WSDW can enter the global ocean easier than WSBW (Naveira Garabato et al., 2002;  
108 Franco et al., 2007) because WSDW is less dense and thus not completely constrained  
109 within the Weddell Basin by the South Scotia Ridge (Gordon et al., 2001; Muench and  
110 Hellmer, 2002). Export of WSBW to the global ocean occurs through upward mixing  
111 with WSDW above or likely through outflows via deep passages (e.g., South Sandwich  
112 Trench; Fig. 1; Ferreira and Kerr, 2017).

113 Recently, Hellmer et al. (2016) performed a comprehensive review study based  
114 on field observations and modelling efforts of meteorology and oceanography of the  
115 Atlantic Sector of the Southern Ocean (i.e. Weddell-Enderby Basin). Those authors  
116 synthesized the Weddell Sea state-of-the-art knowledge regarding the interaction between  
117 the ocean and ice shelves, the physical processes related to water mass formation and  
118 changes, and marine chemistry issues regarding the associated storage of anthropogenic  
119 carbon in that region. Furthermore, as highlighted by Meredith et al. (2014), there is an  
120 essential need to identify and understand the AABW (and its regional varieties) time-  
121 varying formation and export processes, and the controls on properties and flows. For  
122 example, in the Australian Antarctic Sector Wijk and Rintoul (2014) have reported that  
123 the lightning of AABW layer cannot be explained by changes in formation rate alone,  
124 rather resulting from the contribution of less dense AABW varieties. On the other hand,  
125 Azaneu et al. (2013) suggested that changes in formation rate may also have significant  
126 contribution to the contraction of AABW volumes in the Weddell-Enderby Basin. Thus,

127 it is important to understand the causes of AABW properties, export and source-  
128 composition variability (e.g. Fahrbach et al. 2004; 2011), especially at its source zones,  
129 to assess how AABW evolves during time. This may potentially affect its significance  
130 for the global ocean overturning circulation and climate.

131 In this context, this study aims to investigate the temporal variability of the  
132 Weddell Sea deep water masses during the last three decades from 1984 to 2014. Taking  
133 advantage of an extensive dataset, we update the results regarding the temporal variability  
134 of the relative contribution of the deep water masses in the Weddell Sea previously  
135 reported by Kerr et al. (2009a). Those authors analyzed the Weddell Sea deep water mass  
136 structure between 1984 and 1998 and found a 20%-reduction in the WSBW contribution  
137 to the total mixture during that period. Moreover, the present analysis allows for a better  
138 understanding of the primary causes changing the WSBW layer and provides new insights  
139 to the scientific discussion about the causes of the Southern Ocean deep and bottom water  
140 variability and changes.

141

## 142 **2. Data and Methods**

### 143 ***2.1. Hydrographic section data***

144 The potential temperature ( $\theta$ ) and practical salinity ( $S$ ) were selected from two  
145 World Ocean Circulation Experiment (WOCE) hydrographic repeat sections in the  
146 Weddell Sea (Tab. 1; Fig. 1) as follows: (i) section WOCE A12 (also referred to as WOCE  
147 SR2 in the literature) along the Greenwich Meridian, with an irregular sampling period  
148 spanning from 1984 to 2014; and (ii) section WOCE SR4 between Joinville Island and  
149 Kapp Norvegia, with an irregular sampling period spanning between 1989 and 2010.  
150 Section WOCE A12 was restricted here to latitudes higher than  $60^{\circ}\text{S}$ , whereas WOCE  
151 SR4 crossed the entire Weddell Sea (Fig. 1). Those sections were chosen because of their

152 importance to: (i) the regional basin circulation (e.g., Klatt et al., 2005; Meredith et al.,  
 153 2014), (ii) the export routes of deep and bottom waters (e.g., Naveira Garabato et al.,  
 154 2002; Kerr et al., 2012a), and the representativeness for the entire Weddell Basin (e.g.,  
 155 Kerr et al., 2009a; Fahrbach et al., 2011; Jullion et al., 2014). Moreover, here we extend  
 156 the period analyzed by Kerr et al. (2009a) to ~30 years taking advantage of the inclusion  
 157 of five/two additional years at the Greenwich Meridian (WOCE A12) and in the inner  
 158 Weddell Sea (WOCE SR4), respectively (Table 1). We also performed a novel mixing  
 159 scheme approach (see Sect. 2.3) to quantify changes in the source waters of the WSBW.

160  
 161 **Table 1.** Overview of the hydrographic sections used in this study. Details of the observed data can be  
 162 found in Whitworth and Nowlin (1987), Fahrbach et al. (2001, 2004, 2007, 2011), Fahrbach and De Baar  
 163 (2010), Rohardt et al. (2011), van Heuven et al. (2011, 2014), Rohardt and Boebel (2015), and Driemel et  
 164 al. (2017).

Expedition	Cruise Period (dd/mm/yyyy)	WOCE section
AJAX (leg 2)	16/01/1984 – 29/01/1984	A12
ANT-VIII/2	06/09/1989 – 31/10/1989	SR4
ANT-IX/2	16/11/1990 – 30/12/1990	SR4
ANT-X/4	21/05/1992 – 30/07/1992	A12
ANT-X7	03/12/1992 – 23/01/1993	SR4
ANT-XIII/4	17/03/1996 – 20/05/1996	A12 and SR4
ANT-XV/4	28/03/1998 – 23/05/1998	A12 and SR4*
ANT-XVI/2	09/01/1999 – 16/03/1999	A12
ANT-XVIII/3	05/12/2000 – 12/01/2001	A12
ANT-XX/2	24/11/2002 – 23/01/2003	A12
ANT-XXII/3	21/01/2005 – 06/04/2005	A12 and SR4
ANT-XXVII/2	28/11/2010 – 05/02/2011	A12 and SR4
ANT-XXIX/2	02/12/2012 – 14/01/2013	A12
PS89 (ANT-XXX/2)	02/12/2014 – 31/01/2015	A12

165 \*During this year, the section WOCE SR4 was not completely surveyed.

166  
 167 The dataset used was downloaded through the World Ocean Database 2013  
 168 (WOD13; [www.nodc.noaa.gov](http://www.nodc.noaa.gov)) and the Alfred Wegener Institute repository  
 169 ([www.pangaea.de](http://www.pangaea.de)) websites. All observed  $\theta$  and  $S$  data were sampled by high-accuracy  
 170 CTDs and passed through strict data quality control (e.g., Johnson et al., 2013), eventually  
 171 spurious data was manually removed from the compiled dataset. Five different CTD types  
 172 have been used onboard R/V *Polarstern* from 1983 to present days. As the instruments



173 have changed, so have the range, accuracy, stability, resolution, and response of the  
174 sensors. A detailed summary of the instruments' manufacturer specifications of the  
175 instruments as well as the periods they have been on duty is provided in Table 1 and  
176 Figure 1 of Driemel et al. (2017), respectively. For reference, the accuracy limits officially  
177 adopted for WOCE are also listed in Table 1 of Driemel et al. (2017). In general, the  
178 accuracy of  $\theta$ ,  $S$ , and pressure is better than  $\pm 0.003^\circ\text{C}$ ,  $\pm 0.003$  and  $\pm 2$  dbar for the cruises,  
179 respectively (Fahrbach et al., 2011; van Heuven et al., 2014). Data for dissolved oxygen  
180 (DO) was obtained from discrete bottle samples before 2005 and after that by profiling  
181 CTD sensors, which were regularly calibrated against Winkler titrations, with a reported  
182 final accuracy of  $4.5 \mu\text{mol kg}^{-1}$  (van Heuven et al., 2011). Other information regarding  
183 the quality, precision, and calibrations eventually applied to the  $\theta$ ,  $S$ , and DO dataset can  
184 be obtained through the references cited in the caption of Table 1.

185 In addition, we used an ancillary dataset obtained in the Indian Ocean Sector of the  
186 Southern Ocean to discuss the results found (see Section 4). Four repeat occupations  
187 along the section WOCE I6S at  $30^\circ\text{E}$  were obtained via the WOD13 for the years of 1993,  
188 1996, 2006, and 2008. The same dataset was previously analyzed by Couldrey et al.  
189 (2013), where more specific details about the dataset can be found. For this dataset, the  
190 northern limit was restricted to  $60^\circ\text{S}$  and spurious data was manually removed.

191

## 192 **2.2. *Optimum Multiparameter (OMP) analysis***

193 The OMP analysis package (Karstensen and Tomczak, 1999) has been used here  
194 to (i) estimate the vertical distribution, (ii) quantify the mixture, and (iii) elucidate about  
195 the temporal variability of the Weddell Sea deep water masses and the source waters of  
196 WSBW along to hydrographic sections across the Weddell Sea. The method was first  
197 introduced by Tomczak (1981) as an extension of the classical water mass analysis by

198 means of temperature-salinity diagrams (Mamayev, 1975). Mackas et al. (1987),  
199 Tomczak and Large (1989), and Karstensen and Tomczak (1997, 1998) considerably  
200 improved the method allowing for more robust applications. Since then, the OMP analysis  
201 has been successfully applied throughout the global ocean to determine the relative water  
202 mass fractions of contribution on (i) regional (e.g., Huhn et al., 2008; Jenkins et al., 2014;  
203 García-Ibáñez et al., 2015; van Caspel et al., 2015; Dotto et al., 2016), (ii) ocean basin  
204 (e.g., Poole and Tomczak, 1999; Kerr et al., 2009a; Pardo et al., 2012; Santos et al., 2016;  
205 Ferreira and Kerr, 2017), and (iii) global (e.g., Johnson, 2008) scales. The method was  
206 also effectively used to distinguish water mass fractions of mixtures and eventual biases  
207 in Southern Ocean studies using numerical modeling and ocean reanalysis products (e.g.,  
208 Kerr et al., 2009b, 2012b).

209 Briefly, the OMP analysis quantifies the relative fractions of a mixture (or  
210 contributions in % to the total mixture) of distinct source water types (SWT—parameter  
211 values that represent a water mass in its source region) by solving an over-determined  
212 system of linear mixing equations. The following parameters are considered to distinguish  
213 the water mass contributions:  $\theta$ ,  $S$ , and DO. Thus, the linear mixing equations can be  
214 expressed in matrix form as Eq. 1:

$$215 \quad 216 \quad Gx - d = R \quad (1)$$

217 where  $G$  is the SWT matrix, which contains the parameter indices (i.e.  $\theta$ ,  $S$ , and DO) that  
218 represent each of the SWT ( $i=1, \dots, 3$ );  $x$  is the relative contribution from each water  
219 sample; and the vectors  $d$  and  $R$  correspond to the observed dataset and the analysis  
220 residuals, respectively. The only restriction to the method is that the total contribution  
221 from all SWT considered in the mixing scheme must add to 100%. Negative SWT  
222 contributions are not allowed as there is no physical meaning to such numbers. It is also  
223

224 worth mentioning that the OMP analysis was applied in a region of AABW formation  
225 (see Section 2.3). Thus, the increase of one water mass in the mixture of a given year will  
226 necessarily mean that at least one other water mass will decrease its contribution to the  
227 total mixture to assure mass conservation.

228 OMP assumes that all the parameters have the same representativeness. However,  
229 this criterion is not often met because of the influence of environmental variability and  
230 the accuracy of the measurements. Thus, a weighted version of the  $G$  matrix was applied  
231 by including a diagonal matrix  $W$ , which has respective weights for each parameter ( $j=\theta$ ,  
232  $S$ ,  $DO$ ), to correct the external influences. According to Tomczak and Large (1989), the  
233 diagonal matrix  $W$  is obtained by Eq. 2:

234

$$235 \quad W_j = \frac{\sigma_j^2}{\delta_{jmax}} \quad (2)$$

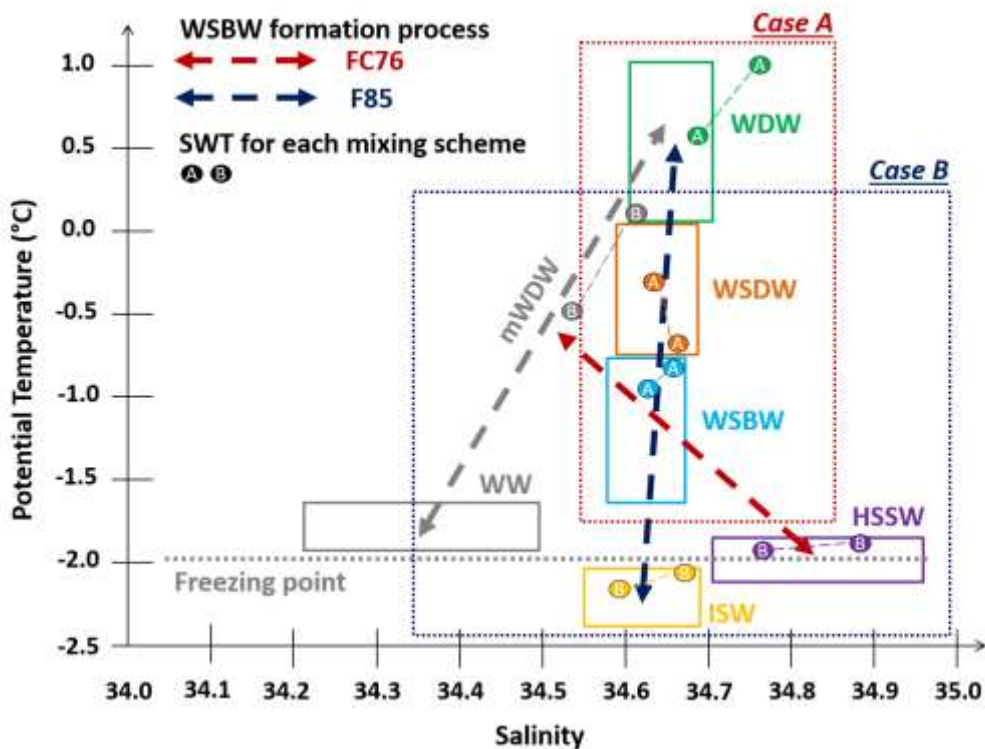
236 where  $\sigma_j^2$  is the variance of each parameter among all SWT and  $\delta_{jmax}$  is the maximum  
237 variance, among the water masses, associated with the same parameter in the source  
238 region. Here, we estimated our own parameter weights instead of arbitrarily define the  
239 values (see caption of Table 2). Mass conservation normally receive the highest weights  
240 found amongst the parameter weights. Mixing equations are weighted to optimize the use  
241 of hydrographic data, so the mass conservation residuals objectively indicate the quality  
242 of the solution, which are normally assumed to be lower than 5–10% (e.g. Tomczak,  
243 1999; Kerr et al. 2009a). Therefore, a low mass conservation residual indicates that the  
244 properties of the water sample are well represented by the SWT considered in the mixing  
245 scheme (Poole and Tomczak, 1999).

247

248

249 **2.3. Deep water mixing schemes and source water types (SWT)**

250 As the study region (i.e., the Weddell Sea) is also a source area of distinct AABW  
 251 varieties, two mixing schemes have been considered here to tackle the proposed aims  
 252 (Fig. 2). The first one (hereafter referred to as *Case A*) follows the same approach used  
 253 by Kerr et al. (2009a), which aims to compute the fractions of mixture of the deep water  
 254 masses that fill the Weddell Basin. In this sense, the following water masses are  
 255 considered: Warm Deep Water (WDW), Weddell Sea Deep Water (WSDW), and  
 256 Weddell Sea Bottom Water (WSBW). This approach allows investigation of the spatial  
 257 distribution and temporal variability of the AABW varieties (WSDW and WSBW) close  
 258 to their main formation area. The reader is referred to inspect Kerr et al. (2009a) for  
 259 additional information regarding the procedures to determine the SWT indices and  
 260 parameter weights defined (Table 2).



261

262 **Figure 2.** Mixing scheme for Weddell Sea Bottom Water (WSBW; light blue rectangle) formation in a  
 263 potential temperature-salinity diagram. The horizontal dotted gray line is the surface freezing temperature.  
 264 The gray and red dashed lines represent the mixing of Warm Deep Water (WDW; green rectangle) with  
 265 Winter Water (WW; gray rectangle) to form modified-WDW (mWDW) and further mixing with High

266 Salinity Shelf Water (HSSW; purple rectangle), representing the Foster and Carmack (1976) process  
 267 (named as FC76). The dark blue dashed line represents WSBW formation by mixing of WDW/mWDW  
 268 with Ice Shelf Water (ISW; yellow rectangle), representing the Foldvik et al. (1985) process (named as  
 269 F85). *Case A* (red dotted rectangle) quantifies the mixture of WDW, Weddell Sea Deep Water (WSDW;  
 270 orange rectangle) and WSBW in the Weddell Sea, whereas *Case B* (dark blue dotted rectangle) informs  
 271 about the source water mass (i.e. mWDW, HSSW and ISW) contribution to form WSBW. The colored dots  
 272 refer to the source water types (SWT) representing the water masses used for each approach (see Table 2).  
 273 (For the interpretation of the references to color in this figure legend, the reader is referred to the web  
 274 version of this article.)  
 275

276 **Table 2.** Range of source water types (SWT) and the parameter weights used in the OMP analyses  
 277 performed, for each mixing scheme, through a Monte Carlo approach in the Weddell Sea. The parameter  
 278 weights, for *Case A*, follow those determined by Kerr et al. (2009), whereas for *Case B* they were  
 279 determined using Eq. 2 and a WOD13 data selection near the western and southern continental margins in  
 280 the Weddell Sea. The dataset extracted to determine the weights for *Case B* was restricted to depths from  
 281 100 m to 600 m.  
 282

SWT Parameters	Case A			Case B				
	WDW	WSDW	WSBW	Weights	mWDW	HSSW	ISW	Weights
$\theta$ [°C]	0.5   1.0	-0.60   -0.30	-0.90   -0.80	11.5	-0.50   0.00	-1.95   -1.91	-2.20   -2.10	18.6
S	34.70   34.75	34.65   34.66	34.64   34.65	11.5	34.54   34.65	34.77   34.87	34.60   34.68	18.6
DO [ $\mu\text{mol L}^{-1}$ ]	208   212	234   248	255   263	11.9 <sup>#</sup>	202.9   251.9	318.4   321.1	321.1   328.6	19.0 <sup>#</sup>

283 <sup>#</sup>Weight applied to the mass conservation.

284

285 The second mixing scheme considered (hereafter referred to as *Case B*) was  
 286 performed for depths greater than 3000 m, which embrace the WSBW core (see for  
 287 instance Fig. 3). In this approach, the SWT precursors of WSBW contributing to the  
 288 mixture were: modified-Warm Deep Water (mWDW), High Salinity Shelf Water  
 289 (HSSW), and Ice Shelf Water (ISW). Thus, the mixing scheme considered in *Case B*  
 290 allows (a) to investigate the contribution changes of the WSBW source water masses and  
 291 (b) to define which source water mass has the main influence in modulating the changes  
 292 of the WSBW contribution throughout the period analyzed (see for instance Fig. 4c). We  
 293 prefer to use a mWDW index instead of separate indices for WW and WDW because of  
 294 (i) the limitation regarding the number of parameters to solve an additional mixing  
 295 equation and (ii) the lack of other potential semi-conservative parameters to be used as  
 296 water mass tracers in some of the cruises. However, additional OMP runs considering  
 297 SWT indices for WW, WDW and one of the shelf water variety indicate negligible

298 contribution of WW ( $< 5\%$ ) to the total mixture (not shown). Considering the *Case B*  
299 applied here, the SWT indices (Tab. 2) were defined using the WOD13 data available  
300 nearby the western and southern continental shelf and shelf-break of the Weddell Sea.  
301 This follows a previous investigation of the water mass properties executed by Huhn et  
302 al. (2008) to better define the SWT indices for HSSW and ISW. Finally, only one SWT  
303 was used to represent each of the water masses considered, independently of the mixing  
304 schemes (Fig. 2; Tab. 2).

305

#### 306 ***2.4. OMP sensitivity analysis***

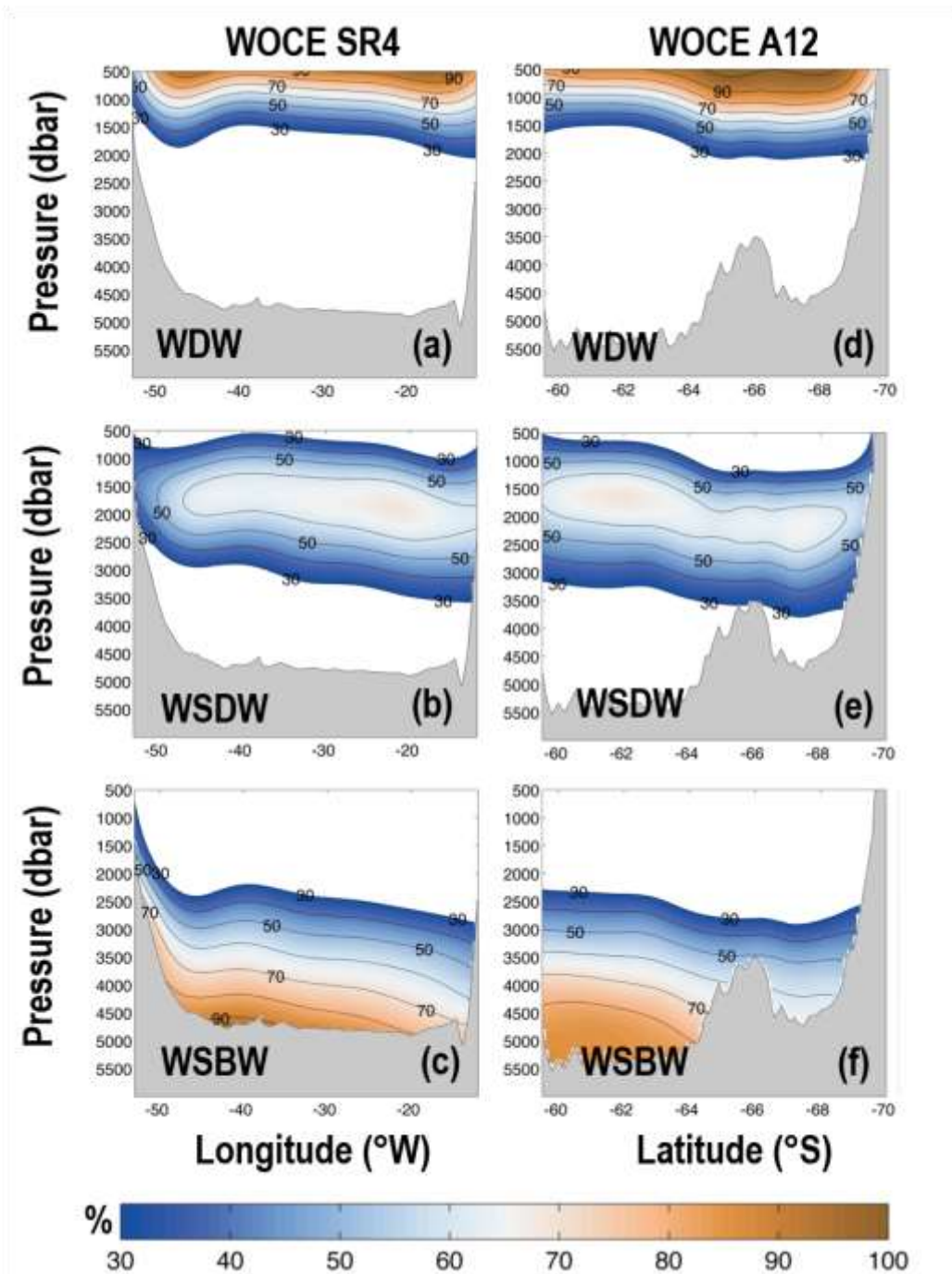
307 The OMP analysis does not consider temporal changes in the SWT definition.  
308 However, the method is widely suitable for identifying the temporal variability of water  
309 masses (e.g. Leffanue and Tomczak 2004; Tomczak and Lieftrink 2005; Kerr et al. 2009a;  
310 Dotto et al. 2016). Thus, to avoid changes in SWT contributions that are related to an  
311 artifact of the method instead of real variations in the SWT fractions, a sensitivity analysis  
312 was performed to evaluate the robustness of the static SWT results. We opted for applying  
313 a Monte Carlo approach to randomly vary the SWT indices between the properties end-  
314 members (Table 2). A total of 100 OMP runs were performed with slightly modified SWT  
315 parameters considering the property range depicted in Table 2. Only the results that had  
316 a mass conservation residual below 10% were considered (Kerr et al., 2009a). In most  
317 cases, differences in the water mass contributions between the numerous OMP runs did  
318 not exceed 5%. Finally, the results presented in the following are the averaged  
319 contributions of all the 100 OMP runs performed. The minimum and maximum water  
320 mass contributions vary between 30-100%, with contribution values above 50% and 60%  
321 used hereafter as criterion to define a water mass layer and core, respectively.

322

### 323 **3. Results**

#### 324 **3.1. Weddell Sea deep water mass structure**

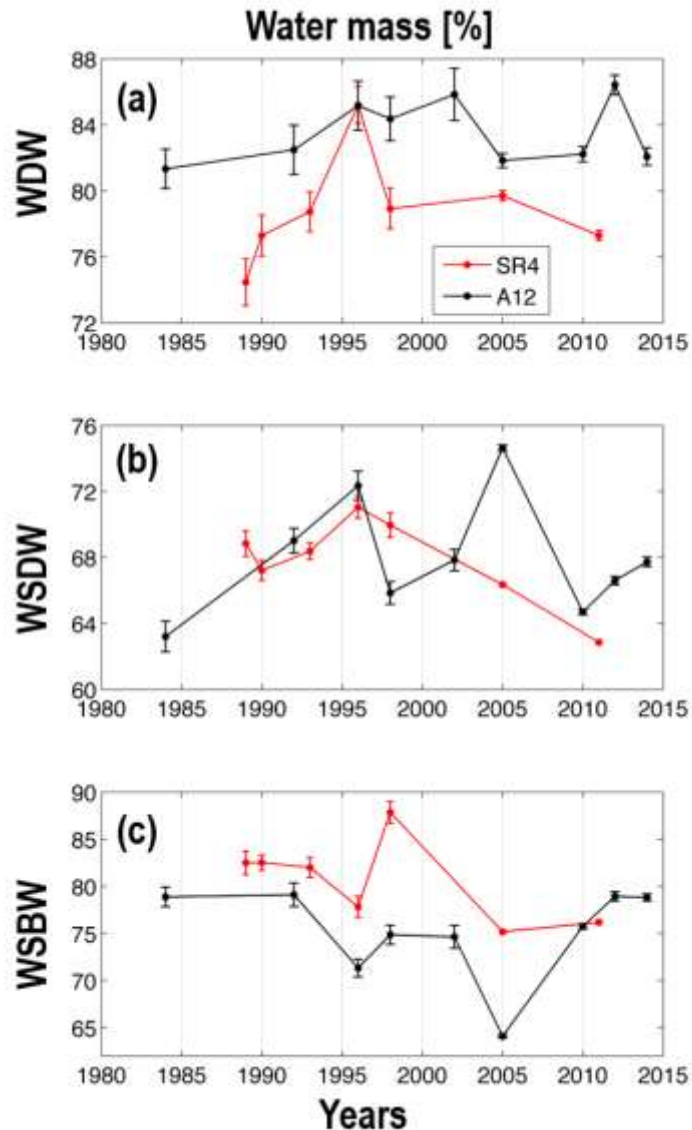
325           The Weddell Sea deep water structure revealed by both hydrographic sections  
326 (WOCE SR4 and A12; Fig. 3) follows that expected for the region (e.g. Kerr et al. 2009a).  
327 The vertical water mass distribution shows: WDW contributing to the mixture in the  
328 upper 1500 m (Fig. 3a, d), WSDW occupies the layer between WDW and WSBW with a  
329 contribution higher than 60% around 2000 m (Fig. 3b, e), and WSBW cascades down the  
330 western continental slope (Fig. 3c) filling the near-bottom layer below 3500 m with a  
331 contribution higher than 60% (Fig. 3c, f). On average, the contributions to the total  
332 mixture between 1989–2011 (1984–2014) in the core of the WDW, WSDW and WSBW  
333 at WOCE SR4 (WOCE A12) were  $79\pm 11\%$  ( $84\pm 13\%$ ),  $68\pm 5\%$  ( $68\pm 5\%$ ),  $81\pm 11\%$   
334 ( $75\pm 9\%$ ), respectively (Fig. 4). The Weddell deep water mass contribution along the  
335 sections observed during each repeat cruise is shown in the Supplementary Material (Figs.  
336 S1 to S3).



337  
338  
339  
340  
341

**Figure 3.** Averaged contribution to the Weddell Sea deep water masses (%) at the WOCE SR4 (left, 1989–2010) and WOCE A12 (right; 1984–2014) sections, respectively. **(a, d)** Warm Deep Water (WDW), **(b, e)** Weddell Sea Deep Water (WSDW), and **(e, f)** Weddell Sea Bottom Water (WSBW). (For the interpretation of the references to color in this figure legend, the reader is referred to the web version of this article.)





342  
 343 **Figure 4.** Time series (1984–2014) of the averaged contribution to the total mixture (%; *Case A*) in the core  
 344 of the water mass (contribution > 60%) of (a) Warm Deep Water (WDW), (b) Weddell Sea Deep Water  
 345 (WSDW), and (c) Weddell Sea Bottom Water (WSBW) on the vertical sections across the Weddell Gyre  
 346 at the Greenwich Meridian (WOCE A12; black line) and in the Weddell Sea from Kapp Norvegia to  
 347 Joinville Island (WOCE SR4; red line). The vertical bars indicate the water mass standard error. (For the  
 348 interpretation of the references to color in this figure legend, the reader is referred to the web version of this  
 349 article.)  
 350

351 **3.2. Weddell Sea deep water mass variability**

352 **3.2.1. Water mass contribution to the total mixture**

353 Temporal changes in the core (contribution > 60%) of the Weddell Sea deep water  
 354 masses show a remarkable degree of interannual variability (Fig. 4). The WDW  
 355 contribution in the Weddell Sea slightly increased (5-10%) for both repeat sections during

356 the whole period (Fig. 4a). A decreasing WSDW contribution is observed after 1996 at  
357 WOCE SR4, while at WOCE A12 the contribution variability was about ~10% (Fig. 4b).  
358 The increased WSDW contribution after 2010 at WOCE A12 is an interesting feature in  
359 the region. Furthermore, WSBW shows a pronounced decrease of ~8-15% between 1989–  
360 1996 and 1984–2005 in the central Weddell Sea and Greenwich Meridian repeat sections  
361 (Fig. 4c), respectively. In fact, the WSBW contribution continues to decrease until 2011  
362 at WOCE SR4, considering that the high contribution observed in 1998 reflects the  
363 western half-section occupation in that particular year. Thereafter, a recovering period is  
364 observed at WOCE A12 for the WSBW contribution, characterized by an increment of  
365 about 15% in the last decade (Fig. 4c).

366

### 367 3.2.2. *Water mass properties variability*

368 To understand the observed variability of the Weddell Sea deep water mass  
369 contributions (section 3.2.1), the time series of the average hydrographic properties of  
370 each water mass were further analyzed using two approaches: (i) a layer based on neutral  
371 density ( $\gamma^n$ ; Jackett & McDougall, 1997) isopycnals (Fig. 5) and (ii) a layer based on the  
372 water mass core (i.e., contribution > 60%; Fig. 6). The first one allows further comparison  
373 with previous studies in the region that used similar methodology to distinguish the water  
374 mass layers (e.g. Fahrbach et al., 2011), whereas the second one allows the investigation  
375 of property changes in the layer of a more homogeneous water mass (or in its most pure  
376 form with less mixture interference from other water masses).

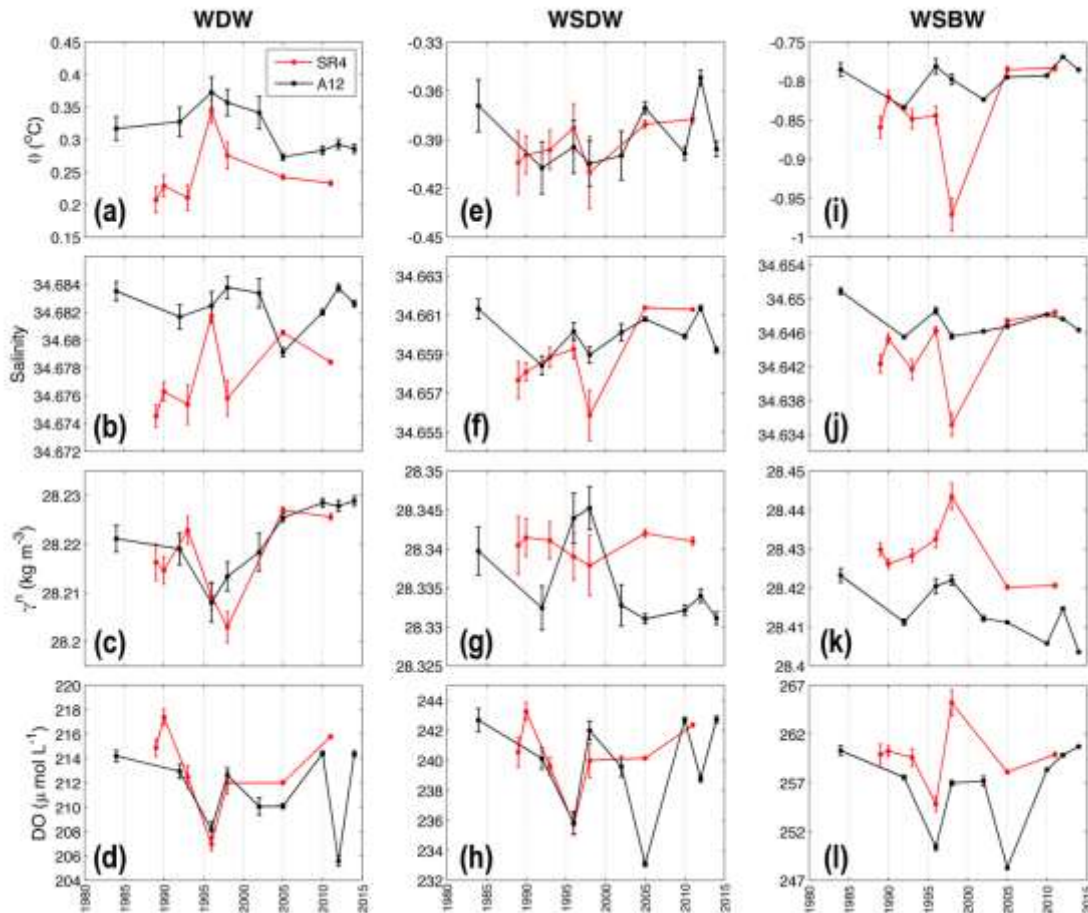
377 Time series of the averaged WDW properties ( $28.1 \geq \gamma^n > 28.27 \text{ kg m}^{-3}$ ; Fig. 5 –  
378 left panels) show a warming of ~0.15°C until 1996 and a cooling of ~0.1°C afterwards,  
379 for both sections (Fig. 5a). Except for the anomalous year of 2005 that showed a drop  
380 (rise) of ~0.04 in the section A12 (SR4), changes in salinity are not pronounced

381 throughout the period analyzed (Fig. 5b). The WDW temperature fluctuations likely  
382 caused slight changes of the average density, with the decreasing temperature after 1996  
383 linked with the densification of the WDW between 1996 and 2014 (Fig. 5c). The DO  
384 variability in the WDW indicates a reduction of  $\sim 16 \mu\text{mol L}^{-1}$  until 1996 and a recovery  
385 afterwards with similar magnitude (Fig. 5d). The year 2012 shows the minimum DO value  
386 recorded in the time series at the WOCE A12 section (Fig. 5d).

387         When analyzing the average WDW properties only at the water mass core (Fig. 6  
388 – left panels), the time series indicates slight changes in temperature ( $\sim 0.1^\circ\text{C}$ ; Fig. 6a) and  
389 no significant fluctuations in salinity ( $\sim 0.004$ ; Fig. 6b), thus leading to small variability  
390 in terms of density (Fig. 6c). On the other hand, DO decreased by  $\sim 8 \mu\text{mol L}^{-1}$  in WOCE  
391 A12 until 2005 (except for the year 1998), while in WOCE SR4 the decrease in DO of  
392 the same magnitude stopped in 1996 (Fig. 6d). Afterwards, one observes a DO increase  
393 of  $\sim 5 \mu\text{mol L}^{-1}$  in the WDW at the WOCE SR4 section. The same magnitude of the DO  
394 increase can be observed at WOCE A12, even with the abrupt drop in DO during the year  
395 2011 (Fig. 6d).

396         Time series of the average WSDW properties ( $28.27 \geq \gamma^n > 28.40 \text{ kg m}^{-3}$ ; Fig. 5 –  
397 center panels) also indicate an interannual variability. Although minor changes were  
398 observed in the average temperature and salinity during the time, it is possible to infer an  
399 increase in temperature and salinity starting after the mid-1980s (Fig. 5e-f). The year 1998  
400 was marked by the lowest temperature and highest salinity in the central Weddell Sea  
401 (however, care should be taken in the interpretation of the patterns of variability as the  
402 WOCE SR4 section was not completely occupied during this year). The oscillations in  
403 the average temperature and salinity are reflected in the variability of WSDW average  
404 density, with an opposing phase between the sections analyzed (Fig. 5g). In the WOCE

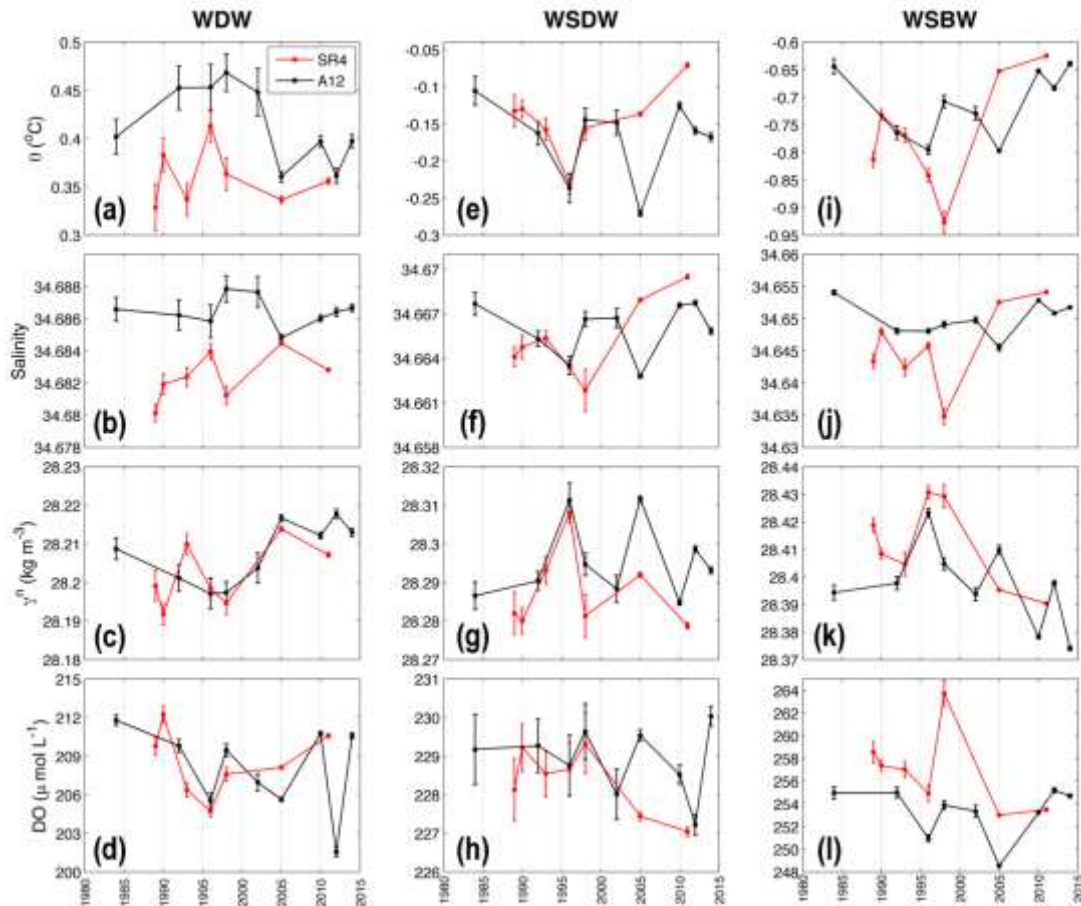
405 A12, less dense WSDW was observed during the 1980s and after the year 2000, and a  
 406 denser variety of WSDW appeared between 1995 and 2000 (Fig. 5g). The opposing  
 407 pattern, with less variability, was observed in WOCE SR4. On the other hand, changes in  
 408 the DO time series occur in phase for both sections and are marked by higher variability  
 409 (Fig. 5h), with a similar pattern to that reported for WDW (Fig. 5d).



410

411 **Figure 5.** Time series (1984–2014) of the average (**top**) potential temperature ( $^{\circ}\text{C}$ ), (**2<sup>nd</sup> row**) salinity, (**3<sup>rd</sup>**  
 412 **row**) neutral density ( $\gamma^n$ ;  $\text{kg m}^{-3}$ ), and (**bottom**) dissolved oxygen (DO;  $\mu\text{mol L}^{-1}$ ) of (**left**) Warm Deep  
 413 Water (WDW;  $28.1 \geq \gamma^n > 28.27 \text{ kg m}^{-3}$ ), (**center**) Weddell Sea Deep Water (WSDW;  $28.27 \geq \gamma^n > 28.40$   
 414  $\text{kg m}^{-3}$ ) and (**right**) Weddell Sea Bottom Water (WSBW;  $\gamma^n \geq 28.40 \text{ kg m}^{-3}$ ) on the sections across the  
 415 Weddell Gyre at the Greenwich Meridian (WOCE A12; black line) and across the Weddell Sea from Kapp  
 416 Norvegia to Joinville Island (WOCE SR4; red line). The neutral density criterion informed was used to  
 417 determine the average of each hydrographic property of each of the Weddell Sea deep water layers. The  
 418 vertical bars indicate the properties standard error. (For the interpretation of the references to color in this  
 419 figure legend, the reader is referred to the web version of this article.)

420



421 **Figure 6.** Time series (1984–2014) of the average (**top**) potential temperature ( $^{\circ}\text{C}$ ), (**2<sup>nd</sup> row**) salinity, (**3<sup>rd</sup>**  
 422 **row**) neutral density ( $\gamma^n$ ;  $\text{kg m}^{-3}$ ), and (**bottom**) dissolved oxygen (DO;  $\mu\text{mol L}^{-1}$ ) in the core (water mass  
 423 contribution > 60%; see Fig. S1–S3) of (**left**) Warm Deep Water (WDW), (**center**) Weddell Sea Deep  
 424 Water (WSDW) and (**right**) Weddell Sea Bottom Water (WSBW) on the sections across the Weddell Gyre  
 425 at the Greenwich Meridian (WOCE A12; black line) and across the Weddell Sea from Kapp Norvegia to  
 426 Joinville Island (WOCE SR4; red line). The vertical bars indicate the properties standard error. (For the  
 427 interpretation of the references to color in this figure legend, the reader is referred to the web version of this  
 428 article.)  
 429

430

431 In contrast to the average WSDW properties based on neutral density layers,  
 432 changes in the WSDW core are more pronounced (Fig. 6 – center panels). The WSDW  
 433 average temperature decreased by  $\sim 0.10\text{--}0.15^{\circ}\text{C}$  until 1996 and increased by  $\sim 0.18^{\circ}\text{C}$   
 434 afterwards (Fig. 6e; obvious in WOCE SR4 and less evident in WOCE A12 because of  
 435 the lowest averaged temperature recorded in 2005), while salinity slightly increased by  
 436  $\sim 0.005$  during the whole period in section SR4 (Fig. 6f). Thus, our results unveil two  
 437 quite distinct periods (Fig. 6g): 1984–1996 (increasing density) and 1996–2014  
 438 (decreasing density). DO decreases by  $\sim 2 \mu\text{mol L}^{-1}$  in WOCE SR4 after the 1990s, while

439 a high degree of DO variability is observed in WOCE A12 with values close to those  
440 observed in the early 1990s for year 2014 (Fig. 6h).

441 The variability observed in the WSBW properties ( $\gamma^n \geq 28.40 \text{ kg m}^{-3}$ ; Fig. 5 – right  
442 panels) is small for average temperature, except for the coldest temperatures recorded in  
443 the year 1998 on WOCE SR4 that reflects the partial occupation of the section (Fig. 5i).  
444 Average salinity decreased by  $\sim 0.004$  at the Greenwich Meridian, whereas changes on  
445 WOCE SR4 reveal small oscillations (Fig. 5j). Despite the year 1998, both temperature  
446 ( $\sim 0.05^\circ\text{C}$ ) and salinity ( $\sim 0.06$ ) increased in the inner Weddell Sea (Fig. 5i-j). The WSBW  
447 average density decreased on WOCE A12 when considering the whole period, whereas  
448 the density increased in the center Weddell Gyre between the start of the time series until  
449 1998 (this increase is also noticeable in the WOCE A12) and decreased afterwards (Fig.  
450 5k). The average DO in WSBW shows a high level of interannual variability (Fig. 5l).  
451 The year 1998 is marked by the highest average DO in WOCE SR4 (again reflecting the  
452 half-section occupation), whereas a pronounced increase in the DO concentration after  
453 2005 is observed in WOCE A12 (Fig. 5l). Thus, one can infer that after 2005 (inclusive)  
454 the WSBW formation recovered, using DO as a proxy to refer to recent water mass  
455 ventilation, i.e., indicating years of strong renewal of the WSBW layer (Fig. 5l).

456 The variability observed only in the WSBW core (Fig. 6 – right panels) shows that  
457 both average temperature ( $\sim 0.15^\circ\text{C}$ ) and salinity ( $\sim 0.005$ ) decreased until 1996 on WOCE  
458 SR4, followed by an increase of  $\sim 0.2^\circ\text{C}$  and  $\sim 0.01$ , respectively (Fig. 6i-j). In spite of the  
459 high variability observed, the WSBW density time series reveals a lightening of that water  
460 mass starting in the mid-1990s (Fig. 6k), in parallel with a reduction of DO concentration  
461 of  $\sim 5\text{-}8 \mu\text{mol L}^{-1}$  during  $\sim 20$  years (1984-2005) in both sections (Fig. 6l). A rapid renewal  
462 of the WSBW layer, occurring within  $\sim 10$  years, after that period is indicated by increased

463 values of DO with the same magnitude previously reported for the beginning of sampling  
464 on section WOCE A12 (Fig. 6l).

465

### 466 **3.3. Weddell Sea Bottom Water sources and changes**

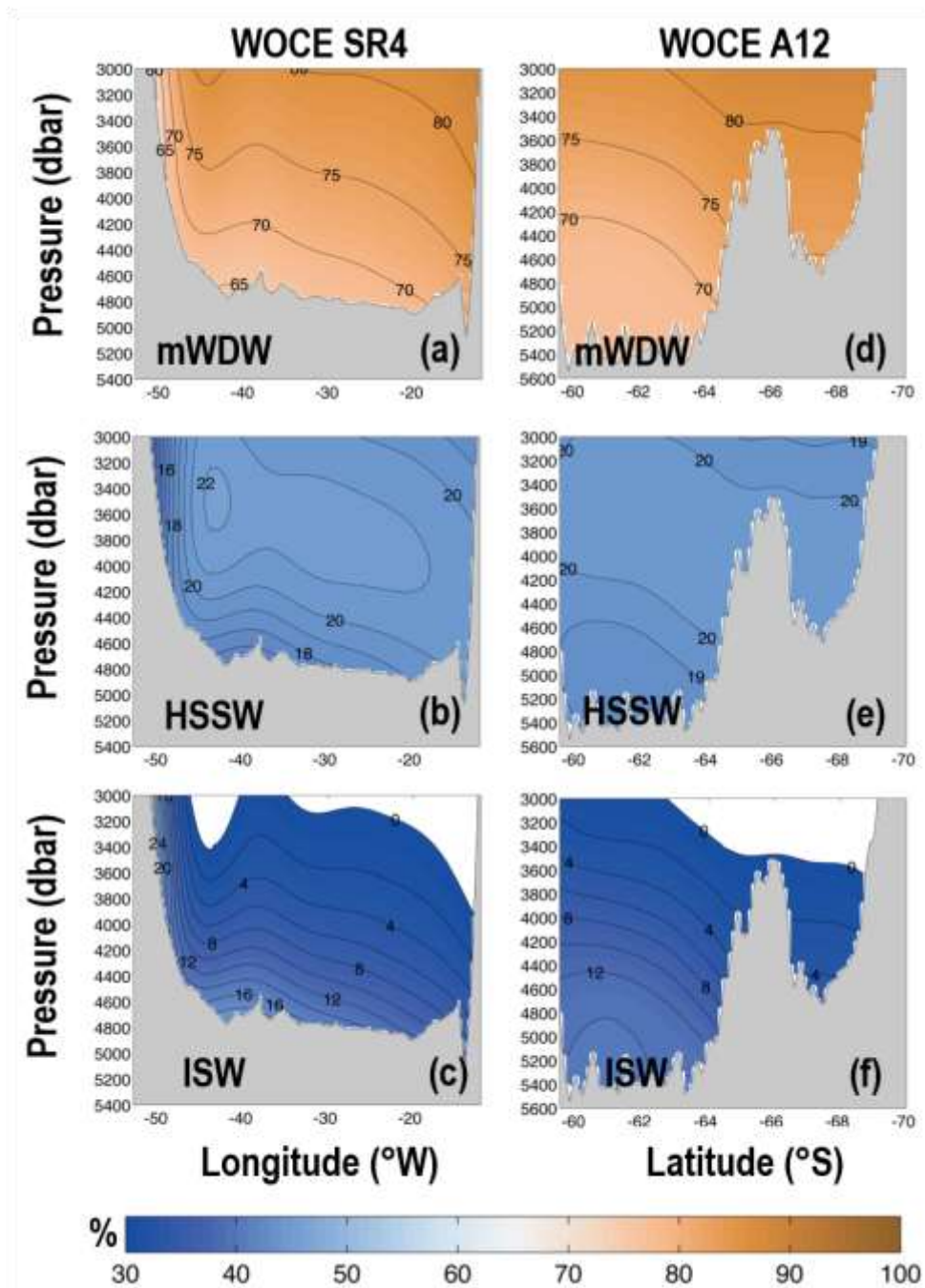
467 The WSBW core (contribution > 60%), considering depths greater than 3000 m,  
468 was composed on average of  $70\pm 5\%$  and  $71\pm 3\%$  of mWDW,  $19\pm 3\%$  and  $20\pm 1\%$  of  
469 HSSW, and  $11\pm 7\%$  and  $9\pm 4\%$  of ISW (Fig. 7) on WOCE SR4 and WOCE A12,  
470 respectively (Fig. 4). As the mWDW and Dense Shelf Waters (sources of the WSBW)  
471 contributions changed throughout the time, it is possible to evaluate which physical  
472 processes potentially influenced the changes of WSBW (Fig. 8).

473 The mWDW contribution increased by ~6-8% through the period analyzed (Fig.  
474 8a), same as reported for WDW quantified in *Case A* (Fig. 4a). Also, the mWDW  
475 contribution decreased by ~4% after 2005 on WOCE A12. The mWDW contribute to  
476 WSBW the most in year 2005 for both sections (Fig. 8a). As the OMP analysis is  
477 constrained by mass conservation in the mixing scheme, the changes observed, when  
478 combining the Dense Shelf Waters contributions (Fig. 8b), are mirrored to mWDW  
479 contribution (Fig. 8a).

480 Although the contribution of both shelf-sources reflects intense interannual  
481 variability, a clear decrease of ~5% of Dense Shelf Waters is observed between 1984–  
482 2005, followed by an increase of ~3% in the section WOCE A12 (Fig. 8b). Separating  
483 the WSBW shelf-sources in HSSW and ISW, one observes an increasing HSSW  
484 contribution of ~3% in the inner Weddell Sea (except for the drop observed in 1998) and  
485 no significant variations at the Prime Meridian (Fig. 8c). On the other hand, the  
486 contribution of ISW decreases between 6-8% for both sections (again excluding the year

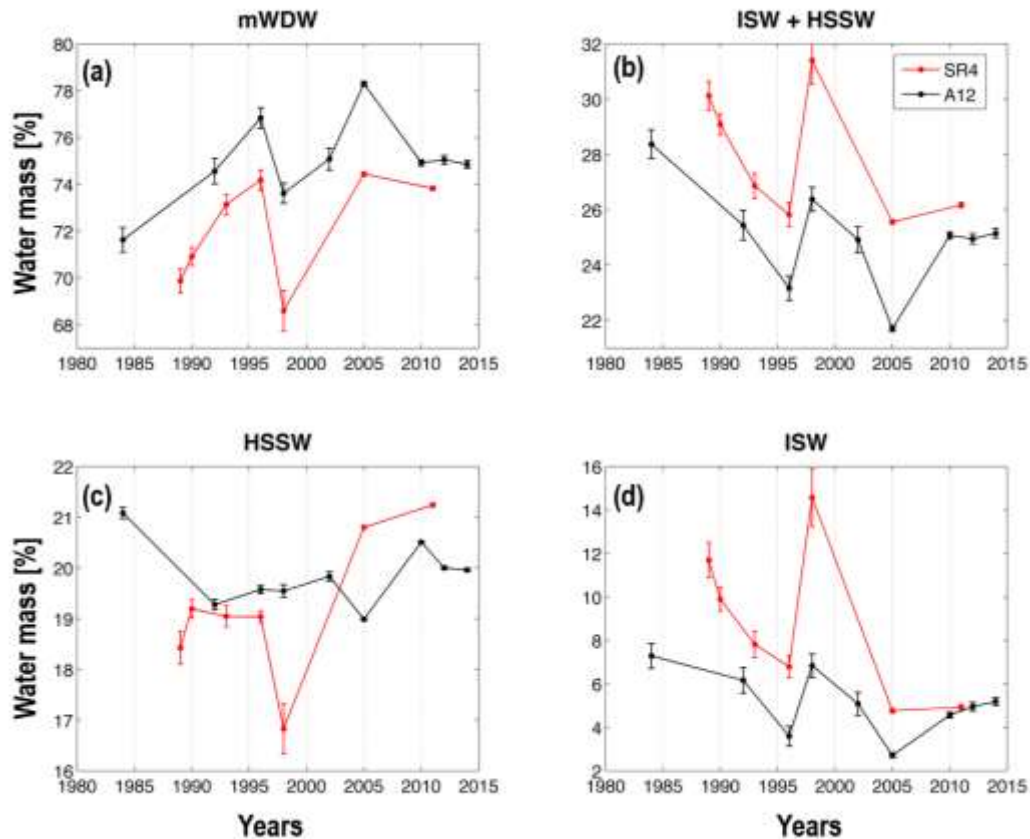


1998 for WOCE SR4) until 2005 (Fig. 8d). After that, the ISW contribution to the WSBW  
 mixture increases by ~2%, which is noticeable on the WOCE A12 section (Fig. 8d).



489  
 490 **Figure 7.** Average contribution (%) of the source water masses of Weddell Sea Bottom Water to the layer  
 491 with contributions > 50% (see Fig. 3c and f) on the sections WOCE SR4 (left panels, 1989–2010) and  
 492 WOCE A12 (right panels; 1984–2014), respectively, (a, d) Warm Deep Water (WDW), (b, e) High Salinity  
 493 Shelf Water (HSSW), and (e, f) Ice Shelf Water (ISW). (For the interpretation of the references to color in  
 494 this figure legend, the reader is referred to the web version of this article.)  
 495





496 **Figure 8.** Time series (1984–2014) of the average source water mass contribution - (a) modified-Warm  
 497 Deep Water (mWDW), (b) Dense Shelf Waters (merged contribution of HSSW and ISW), (c) High Salinity  
 498 Shelf Water (HSSW), and (d) Ice Shelf Water (ISW) to the total mixture (%; *Case B*) in the Weddell Sea  
 499 Bottom Water (Fig. 3c and f) on the section across the Weddell Gyre at the Greenwich Meridian (WOCE  
 500 A12; black line) and across the Weddell Sea from Kapp Norvegia to Joinville Island (WOCE SR4; red  
 501 line). The vertical bars indicate the water mass standard error. (For the interpretation of the references to  
 502 color in this figure legend, the reader is referred to the web version of this article.)  
 503  
 504

#### 505 4. Discussion and Conclusion

506 The Weddell Sea deep water mass structure presented in Figure 3 agrees with that  
 507 previously described by Kerr et al. (2009a) as expected, because both studies used the  
 508 same methodology and datasets overlap during part of the time series. However, the use  
 509 of a more appropriate sensitive analysis here, through a Monte Carlo approach varying  
 510 the SWT, causes changes in the average contribution and the depth-limits of WSDW  
 511 boundary with other water masses when compared to the previous study. Thus, the  
 512 WDW/WSDW and WSDW/WSBW boundaries changed approximately by 500 m from  
 513 those previously reported by Farhbach et al. (2004; 2011). The authors split the water

514 mass layers in the Weddell Sea using the isopycnal (isotherm) boundary of  $28.27 \text{ kg m}^{-3}$   
515 ( $0 \text{ }^\circ\text{C}$ ) and  $28.40 \text{ kg m}^{-3}$  ( $-0.7 \text{ }^\circ\text{C}$ ), which changes the depth of the water mass mixing  
516 zone between the studies. However, the combined use of temperature, salinity, and DO,  
517 to distinguish the layer of the purest form of the water masses (i.e., its high percentage of  
518 mixture), reveals further important aspects regarding how a particular water mass evolves  
519 through time. That was sometimes masked using the above parameter thresholds. The  
520 temporal variability observed in the contribution to Weddell Sea deep waters (Sect. 3.2.1)  
521 is likely caused by a combination of changes in (i) the source water mass properties  
522 (Meredith et al., 2011; Azaneu et al., 2013; Schmidtke et al., 2014), (ii) the Weddell Gyre  
523 circulation and dynamics (Meredith et al., 2008; Jullion et al., 2014), and (iii) the  
524 production and export of Dense Shelf Waters from the shelf (Kerr et al. 2012a; Heywood  
525 et al., 2014). In fact, shifts in WSBW hydrographic properties towards less dense varieties  
526 (Figs. 5k) likely equate to less WSBW being produced over time, which is further  
527 supported by the decreasing of DO concentration (i.e., less ventilation) in the bottom  
528 layer (Fig. 6k) of the Weddell Sea.

529         The increasing contribution of WDW (Fig. 4a) during the three decades analyzed  
530 is possibly reflecting the intensification of the Southern Ocean winds driven by the  
531 positive long-term trend of the Southern Annular Mode (Jullion et al., 2010). That  
532 mechanism may play a role on the southward displacement of the fronts of the Antarctic  
533 Circumpolar Current (Sokolov and Rintoul, 2009) and on the intensity of mesoscale  
534 eddies in the Southern Ocean (Meredith, 2016). Both processes can possibly influence  
535 the inflow of Circumpolar Deep Water (CDW—a water mass precursor of WDW) into  
536 the Weddell Sea. Thus, the processes may allow the WDW contribution to increase in  
537 phase and at similar rates both along the Prime Meridian and in the inner Weddell Sea  
538 (Fig. 4a; Table 3). It is also important to highlight that the temporal changes in the WDW

539 layer are affected by a mixture of different CDW-inflows from the Antarctic Circumpolar  
540 Current and recirculated-WDW in the Prime Meridian region (Ryan et al., 2016). Hence,  
541 the WDW core gradually merges and becomes more homogeneous towards the west  
542 (Leach et al, 2011), such as observed by the property time series (Fig. 6 – left panels). In  
543 addition, the WDW increased availability within the Weddell Gyre during the three  
544 decades analyzed (Fig. 4a) has changed the WSBW layer, which now unveils a higher  
545 percentage of the former as part of its composition (Fig. 8a). In fact, that observation  
546 agrees with the reported declining ventilation of the Antarctic deep and bottom waters  
547 (Huhn et al., 2008), which was simultaneously manifested in the Weddell Sea by a  
548 decrease of ~20% in the WSBW contribution (Kerr et al. 2009a), the AABW volume  
549 contraction (Azaneu et al., 2013), and a decreasing trend in DO for the bottom layer (van  
550 Heuven et al., 2014).

551         The temporal changes of the WSDW contribution (Fig. 4b) reveal a marked  
552 interannual variability (sometimes varying the contribution up to ~10%), which is likely  
553 driven by small changes in the rate its precursor water masses mix during the formation  
554 process (Daae et al., 2009), but also due to changes in the internal diapycnal mixing  
555 (Heywood et al., 2002; Sloyan, 2005) and Southern Ocean circulation (Naveira Garabato  
556 et al., 2014). This behavior is more obvious on the WOCE A12 section as that region is  
557 more dynamically active because of both the steep bathymetry and the vicinity to the  
558 inflow of CDW into the Weddell Sea (~20-30°E; e.g. Gouretski and Danilov, 1993;  
559 Schröder and Fahrbach, 1999; Ryan et al., 2016). Furthermore, the rapid renewal of the  
560 WSBW layer observed after 2005 at the Prime Meridian (Fig. 4c) is also seen in the  
561 WSDW layer after 2010 (Fig. 4b). [The ~5 years lag can be an indicator for the mixing](#)  
562 [time scale between WSDW and WSBW, although further investigation is needed due to](#)

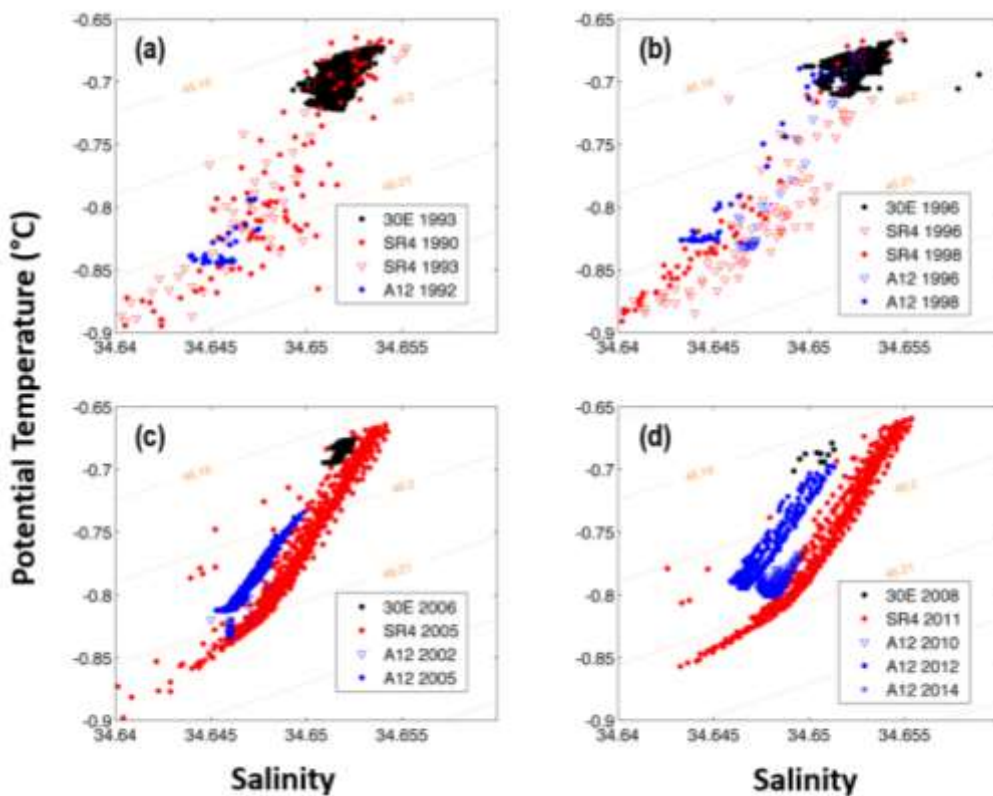
563 the relatively sparse temporal resolution combined with the strong temporal variability of  
564 the properties of those water masses.

565 The decreasing WSDW contribution in WOCE SR4 is within the same range of  
566 the temporal variability as reported for the Prime Meridian (Fig. 4b). This suggests that  
567 the Weddell Gyre circulation can damp temporal changes within the Weddell Sea, but it  
568 also demonstrates that WSDW (the most voluminous water mass filling the Weddell  
569 Basin) is not completely matured. In fact, Robertson et al. (2002) pointed out that,  
570 although the average WSDW potential temperature between 1500 m and 3500 m was  
571 higher in the 1990s than in the 1970s, high variability in the data prevented the  
572 identification of a well-defined temporal trend. Moreover, changes in salinity were not  
573 observed in the deep layer of the Weddell Sea ( $\sigma^{\theta} > 28.27 \text{ kg m}^{-3}$ ) using a dataset of ~50  
574 years (1958–2010; Azaneu et al., 2013), which is an intriguing observation given the  
575 recent freshening of AABW varieties and AABW shelf-sources reported for sites all  
576 around the Antarctic continent (Aoki et al., 2005; Rintoul, 2007; Hellmer et al., 2011;  
577 Jullion et al., 2013; Dotto et al., 2016). Hence, a swifter circulation in the Weddell Sea  
578 (Meredith et al., 2011) can also contribute to an enhanced export of WSDW, newly  
579 formed in the northwestern Weddell Sea. That young water mass potentially carries out  
580 of the Weddell Sea the freshening signal resulting from changes in Dense Shelf Waters  
581 properties (Azaneu et al., 2013) due to ocean-ice interactions (Cook et al., 2005; Pritchard  
582 and Vaughan, 2007; Chen et al., 2008; Rignot et al., 2008; Cook et al., 2016). Thus,  
583 preventing those time changes in the properties of the WSDW sources leads to a more  
584 consistent impact on their contribution to the total mixture in the inner Weddell Sea.  
585 Moreover, the time series currently available are not long enough yet to allow for a  
586 distinction of the signals and further conclusions on the drivers of the WSDW temporal  
587 variability.

588 Changes in the WSBW contribution (Fig. 4c) agree with the ~20% decrease  
589 previously reported by Kerr et al. (2009a) until the end of the 1990s, but the WSBW  
590 formation strength recovers afterwards. The pattern reversal is clearly visible by the  
591 increased WSBW contribution after 2005 in WOCE A12, but not apparently manifested  
592 in the inner Weddell Sea. However, the vigorous increase of WSBW at the Prime  
593 Meridian indicates that other dense bottom water sources are influencing the region (e.g.  
594 Couldrey et al, 2013). In this context, the changes observed in the WSBW precursors  
595 (Fig. 8) indicate that Dense Shelf Waters are responsible for modulating the WSBW  
596 variability. This is particularly true because the mWDW contribution to the WSBW layer  
597 (Fig. 8a) and the strength of the WDW core in the Weddell Sea (Fig. 4a) both have  
598 increased throughout the time series. The Dense Shelf Waters (Fig. 8b) contribution  
599 unveils a behavior with similar temporal changes as in the WSBW contribution (Fig. 4c)  
600 and changes in the DO content of the WSBW layer (Fig. 6l). It is interesting to note that  
601 even the Dense Shelf Waters modulate the WSBW temporal changes when separating the  
602 contribution into HSSW and ISW. The variability of the WSBW in WOCE SR4 (Fig. 4c)  
603 is mostly driven by the increasing (decreasing) contribution of HSSW (ISW) (Fig. 8c),  
604 whereas ISW modulates the WSBW changes in WOCE A12 after 2005 since HSSW  
605 monotonically changes through time (Fig. 8d).

606 The newly-formed WSBW, present in the region of WOCE A12, likely results  
607 from an increasing contribution of other AABW varieties formed in the Indian Sector of  
608 the Southern Ocean, being advected towards the Prime Meridian as previously proposed  
609 by Meredith et al. (1999; 2000) and Jullion et al. (2014). The potential temperature-  
610 salinity diagram (Fig. 9), considering AABW varieties with  $\gamma^n \geq 28.40 \text{ kg m}^{-3}$  at 30°E, 0°,  
611 and the inner Weddell Sea, shows that the AABW variety marked as WSBW on WOCE  
612 A12 is derived from the Indian Ocean-variety of AABW after 2005 (Fig. 9c and d), which

613 has a density different from the varieties formed within the Weddell Sea. However, no  
 614 distinction of the AABW sources is evident during the 1990s, because AABW varieties  
 615 at the Prime Meridian and in the Indian Sector followed roughly the same isopycnals (Fig.  
 616 9a and b). It is worth mentioning that both the different vertical resolution of each datasets  
 617 (e.g., bottle and CTD) used and the possible inter-cruise systematic differences have a  
 618 negligible effect on this conclusion (e.g., salinity differences are within the same range  
 619 of the deviation of the label standard seawater salinity in laboratory measurements).  
 620 Therefore, the observations indicate that prior to 2005 the bottom waters were well-mixed  
 621 in the region and/or no pulses of AABW of Indian Ocean origin occurred during that  
 622 period.



623 **Figure 9.** Potential temperature-salinity diagrams considering the near-bottom layer ( $\gamma^n \geq 28.4 \text{ kg m}^{-3}$ ) and  
 624 latitude greater than  $60^\circ\text{S}$  at the WOCE SR4 (inner Weddell Sea; red symbols), WOCE A12 (Prime  
 625 Meridian; blue symbols), and WOCE I6S ( $30^\circ\text{E}$ ; black dots) repeat sections. The dataset used for WOCE  
 626 SR4 and WOCE A12 is the same used to perform the OMP analysis. The year of the measurement is  
 627 indicated by the legend for each respective section, grouped in nearest sampling years: (a) 1990–1993, (b)  
 628 1996–1998, (c) 2002–2006, and (d) 2008–2014. The isopycnals refers to  $\sigma_4$ . (For the interpretation of the  
 629 references to color in this figure legend, the reader is referred to the web version of this article.)  
 630  
 631

632 In addition, the source water mass contributions to WSBW are redefined here to  
633 be composed by a mixture of  $71\pm 4\%$  of mWDW,  $19\pm 2\%$  of HSSW, and  $10\pm 6\%$  of ISW  
634 (Fig. 7) for the whole Weddell Sea, with almost no difference between both regions  
635 analyzed. These results update the proportion of the sources forming WSBW, previously  
636 estimated to be approximately 65% of WDW and 35% of Dense Shelf Waters (Gill, 1973;  
637 Carmack, 1974). Also, assuming that Dense Shelf Waters are the youngest water masses  
638 of the WSBW precursors, our results corroborate with earlier estimates that 12% to 30%  
639 of the bottom waters in the Weddell Sea are newly-formed (Carmack and Foster, 1975).

640 In summary, extending the time series analysis of Weddell Sea deep and bottom  
641 water properties to around three decades of investigation (even considering the sparse  
642 temporal resolution) allows us to better understand the WSBW origin in the Weddell Sea  
643 and how it has been evolved (transformed/modified) over time. This study shows that  
644 shifts in WSBW properties towards less dense varieties in the Weddell Sea likely equate  
645 to less WSBW being produced over time. The decline of WSBW volume observed until  
646 the 1990s ceased around 2005 and likely recovered thereafter (particularly in the WOCE  
647 A12 region, due to pulses of AABW from the Indian Ocean). The increase of the WSBW  
648 contribution results from changes in the proportion of WDW and Dense Shelf Waters,  
649 while the latter drive and modulate the recent WSBW variability. As a result, WSBW  
650 present in the Weddell Basin is now composed by 71% of WDW and 29% of Dense Shelf  
651 Waters.

652 Finally, the distinction between the AABW varieties within the entire Southern  
653 Ocean is still a complex issue to be solved due to the proximity of their property values.  
654 However, as particular ocean-ice processes with different time scales are responsible for  
655 modifying the regional varieties of AABW in diverse ways, further efforts should be  
656 taken to correctly interpret the signals of recent AABW warming and freshening that

657 spread towards the global ocean (Bindoff and Hobbs, 2013). In this context, the Southern  
658 Ocean environment (mostly during austral winter when AABW formation in particular  
659 occurs) imposes a barrier for comprehensive synoptic observations around the continent  
660 even in the light of modern technologies and techniques. Nevertheless, some progress has  
661 been achieved to observe the ocean under the ice as this task has been receiving special  
662 attention from the international community (Meredith et al., 2013; 2015). Unfortunately,  
663 ocean models and reanalysis products normally lack to properly represent the AABW  
664 layer as well as its properties and formation processes (Kerr et al. 2009b; Kerr et al.,  
665 2012a, b; Azaneu et al., 2014; Dotto et al., 2014). Nevertheless, a recent investigation on  
666 the representation of deep convection occurring in ocean reanalysis products revealed that  
667 the mechanism of AABW formation in the Indian Sector of the Southern Ocean is  
668 plausible by combining both continental shelf convection and the export of Dense Shelf  
669 Waters to the open ocean (Aguiar et al., 2017). These findings indicate that observations  
670 and modeling should be used together to fill the gaps and better understand the processes  
671 controlling the formation and variability of AABW regional varieties.

672

## 673 **5. Acknowledgements**

674 This work is dedicated to the memory of Eberhard Fahrback, without his vision  
675 and efforts, this most valuable data set of the Weddell Sea covering more than three  
676 decades would not exist. This study provides a contribution to the activities of the  
677 Brazilian High Latitudes Oceanography Group (GOAL), which is part of the Brazilian  
678 Antarctic Program (PROANTAR). GOAL has been funded by and/or has received  
679 logistical support from the Brazilian Ministry of the Environment (MMA), the Brazilian  
680 Ministry of Science, Technology, Innovation and Communication (MCTIC), and the  
681 Council for Research and Scientific Development of Brazil (CNPq) through grants from



682 the Brazilian National Institute of Science and Technology of Cryosphere (INCT-  
683 CRIOSFERA; CNPq grants n° 573720/2008-8 and 465680/2014-3), NAUTILUS (CNPq  
684 grant n° 405869/2013-4), and CAPES/CMAR2 (CAPES grant n° 23038.001421/2014-30)  
685 projects. R. Kerr and M. M. Mata acknowledge CNPq researcher grants n° 302604/2015-  
686 4 and 306896/2015-0, respectively. T. S. Dotto was funded by a CNPq PhD grant n°  
687 232792/2014-3. We are grateful for the constructive comments provided by two  
688 anonymous reviewers which substantially improved the manuscript.

689

## 690 **6. References**

- 691 Aguiar, W.C., Mata, M. M. & Kerr, R., (2017; accepted for OS). On the deep convection  
692 events and Antarctic Bottom Water formation in ocean reanalysis products. *Ocean*  
693 *Science Discussions*, doi:10.5194/os-2017-9.
- 694
- 695 Aoki, S., Rintoul, S. R., Ushio, S., Watanabe, S., & Bindoff, N. L. (2005). Freshening of  
696 the Adélie Land Bottom water near 140 E. *Geophysical Research Letters*, 32(23).
- 697
- 698 Azaneu, M., Kerr, R., Mata, M. M., & Garcia, C. A. (2013). Trends in the deep Southern  
699 Ocean (1958–2010): Implications for Antarctic Bottom Water properties and volume  
700 export. *Journal of Geophysical Research: Oceans*, 118(9), 4213-4227.
- 701
- 702 Azaneu, M., Kerr, R., & Mata, M. M. (2014). Assessment of the representation of  
703 Antarctic Bottom Water properties in the ECCO2 reanalysis. *Ocean Science*, 10(6), 923.
- 704
- 705 Bindoff, N. L., & Hobbs, W. R. (2013). Oceanography: Deep ocean freshening. *Nature*  
706 *Climate Change*, 3(10), 864-865.
- 707
- 708 Carmack, E. C. (1974). A quantitative characterization of water masses in the Weddell  
709 Sea during summer. *Deep Sea Research and Oceanographic Abstracts*. Vol. 21, No. 6,  
710 pp. 431-443.
- 711
- 712 Carmack, E. C., & Foster, T. D. (1975a). On the flow of water out of the Weddell Sea.  
713 *Deep Sea Research and Oceanographic Abstracts*. Vol. 22, No. 11, pp. 711-724.
- 714
- 715 Carmack, E. C., & Foster, T. D. (1975b). Circulation and distribution of oceanographic  
716 properties near the Filchner Ice Shelf. *Deep Sea Research and Oceanographic Abstracts*  
717 Vol. 22, No. 2, pp. 77-90.
- 718
- 719 Chen, J. L., Wilson, C. R., Tapley, B. D., Blankenship, D., & Young, D. (2008). Antarctic  
720 regional ice loss rates from GRACE. *Earth and Planetary Science Letters*, 266(1), 140-  
721 148.
- 722
- 723 Comiso, J. C. and Gordon, A. L.: Recurring polynyas over the Cosmonaut Sea and the  
724 Maud Rise, *J. Geophys. Res.-Ocean.*, 92, 2819–2833,  
725 <https://doi.org/10.1029/JC092iC03p02819>, 1987.
- 726
- 727 Cook, A. J., Fox, A. J., Vaughan, D. G., & Ferrigno, J. G. (2005). Retreating glacier fronts  
728 on the Antarctic Peninsula over the past half-century. *Science*, 308(5721), 541-544.
- 729
- 730 Cook, A. J., Holland, P. R., Meredith, M. P., Murray, T., Luckman, A., & Vaughan, D.  
731 G. (2016). Ocean forcing of glacier retreat in the western Antarctic Peninsula. *Science*,  
732 353(6296), 283-286.
- 733
- 734 Couldrey, M. P., Jullion, L., Naveira Garabato, A. C., Rye, C., Herráiz-Borreguero, L.,  
735 Brown, P. J., ... & Speer, K. L. (2013). Remotely induced warming of Antarctic Bottom  
736 Water in the eastern Weddell gyre. *Geophysical Research Letters*, 40(11), 2755-2760.
- 737

738 Daae, K. L., Fer, I., & Abrahamsen, E. P. (2009). Mixing on the continental slope of the  
739 southern Weddell Sea. *Journal of Geophysical Research: Oceans*, 114(C9).  
740

741 De Lavergne, C., Palter, J. B., Galbraith, E. D., Bernardello, R., & Marinov, I. (2014).  
742 Cessation of deep convection in the open Southern Ocean under anthropogenic climate  
743 change. *Nature Climate Change*, 4(4), 278-282.  
744

745 Dotto, T. S., Kerr, R., Mata, M. M., Azaneu, M., Wainer, I. E. K. C., Fahrbach, E., &  
746 Rohardt, G. (2014). Assessment of the structure and variability of Weddell Sea water  
747 masses in distinct ocean reanalysis products. *Ocean Science*, 10, 523–546, 2014, 10, 523-  
748 546.  
749

750 Dotto, T. S., Kerr, R., Mata, M. M., & Garcia, C. A. (2016). Multidecadal freshening and  
751 lightening in the deep waters of the Bransfield Strait, Antarctica. *Journal of Geophysical  
752 Research: Oceans*, 121(6), 3741-3756.  
753

754 Driemel, A., Fahrbach, E., Rohardt, G., Beszczynska-Möller, A., Boetius, A., Budéus,  
755 G., Cisewski, B., Engbrodt, R., Gauger, S., Geibert, W., Geprägs, P., Gerdes, D.,  
756 Gersonde, R., Gordon, A. L., Grobe, H., Hellmer, H. H., Isla, E., Jacobs, S. S., Janout,  
757 M., Jokat, W., Klages, M., Kuhn, G., Meincke, J., Ober, S., Østerhus, S., Peterson, R. G.,  
758 Rabe, B., Rudels, B., Schauer, U., Schröder, M., Schumacher, S., Sieger, R., Sildam, J.,  
759 Soltwedel, T., Stangeew, E., Stein, M., Strass, V. H., Thiede, J., Tippenhauer, S., Veth,  
760 C., von Appen, W.-J., Weirig, M.-F., Wisotzki, A., Wolf-Gladrow, D. A., and Kanzow,  
761 T.: From pole to pole: 33 years of physical oceanography onboard R/V Polarstern, *Earth  
762 Syst. Sci. Data*, 9, 211-220, <https://doi.org/10.5194/essd-9-211-2017>, 2017.  
763

764 Fahrbach, E., Harms, S., Rohardt, G., Schröder, M., & Woodgate, R. A. (2001). Flow of  
765 bottom water in the northwestern Weddell Sea. *Journal of Geophysical Research: Oceans*,  
766 106(C2), 2761-2778.  
767

768 Fahrbach, E., Hoppema, M., Rohardt, G., Schröder, M., & Wisotzki, A. (2004). Decadal-  
769 scale variations of water mass properties in the deep Weddell Sea. *Ocean Dynamics*,  
770 54(1), 77-91.  
771

772 Fahrbach, E., Rohardt, G., and Sieger, R.: 25 Years of Polarstern hydrography (1982–  
773 2007), WDC-MARE Reports 5, Alfred-Wegener-Institut, Bremerhaven, 94 pp., 2007.  
774

775 Fahrbach, E. and De Baar, H.: The Expedition of the Research Vessel Polarstern to the  
776 Antarctic in 2008 (ANT-XXIV/3). *Bericht zur Polar- und Meeresforschung*, Vol. 606,  
777 Alfred-Wegener-Institut, Bremerhaven, 228 pp., 2010.  
778

779 Fahrbach, E., Hoppema, M., Rohardt, G., Boebel, O., Klatt, O., & Wisotzki, A. (2011).  
780 Warming of deep and abyssal water masses along the Greenwich meridian on decadal  
781 time scales: The Weddell gyre as a heat buffer. *Deep Sea Research Part II: Topical Studies  
782 in Oceanography*, 58(25), 2509-2523.  
783

784 Ferreira, M. L., & Kerr, R. (2017). Source water distribution and quantification of North  
785 Atlantic Deep Water and Antarctic Bottom Water in the Atlantic Ocean. *Progress in  
786 Oceanography*, 153, 66-83.  
787

788 Foldvik, A., Gammelsrød, T., & Tørresen, T. (1985). Circulation and water masses on the  
789 southern Weddell Sea shelf. *Oceanology of the Antarctic continental shelf*, 5-20.  
790

791 Foster, T. D., & Carmack, E. C. (1976a). Frontal zone mixing and Antarctic Bottom  
792 Water formation in the southern Weddell Sea. *Deep Sea Research and Oceanographic*  
793 *Abstracts*. Vol. 23, No. 4, pp. 301-317  
794

795 Foster, T. D., & Carmack, E. C. (1976b). Temperature and salinity structure in the  
796 Weddell Sea. *Journal of Physical Oceanography*, 6(1), 36-44.  
797

798 Franco, B. C., Mata, M. M., Piola, A. R., & Garcia, C. A. (2007). Northwestern Weddell  
799 Sea deep outflow into the Scotia Sea during the austral summers of 2000 and 2001  
800 estimated by inverse methods. *Deep Sea Research Part I: Oceanographic Research*  
801 *Papers*, 54(10), 1815-1840.  
802

803 Garcia-Ibanez, M. I., Pardo, P. C., Carracedo, L. I., Mercier, H., Lherminier, P., Rios, A.  
804 F., & Perez, F. F. (2015). Structure, transports and transformations of the water masses  
805 in the Atlantic Subpolar Gyre. *Progress in Oceanography*, 135, 18-36.  
806

807 Gill, A. E. (1973). Circulation and bottom water production in the Weddell Sea. *Deep Sea*  
808 *Research and Oceanographic Abstracts*. Vol. 20, No. 2, pp. 111-140.  
809

810 Gordon, A. L. (1978). Deep Antarctic convection west of Maud Rise. *Journal of Physical*  
811 *Oceanography*, 8(4), 600-612.  
812

813 Gordon, A. L. (2014). Oceanography: Southern Ocean polynya. *Nature Climate Change*,  
814 4(4), 249-250.  
815

816 Gordon, A. L., Huber, B. A., Hellmer, H. H., & Field, A. (1993). Deep and bottom water  
817 of the Weddell Sea's western rim. *Science*, 262(5130), 95-98.  
818

819 Gordon, A. L., Visbeck, M., & Comiso, J. C. (2007). A possible link between the Weddell  
820 Polynya and the Southern Annular Mode. *Journal of Climate*, 20(11), 2558-2571.  
821

822 Gordon, A., Visbeck, M., & Huber, B. (2001). Export of Weddell Sea deep and bottom  
823 water. *Journal of Geophysical Research-Oceans*, 106, 9005-9017.  
824

825 Gouretski, V. V., & Danilov, A. I. (1993). Weddell Gyre: structure of the eastern  
826 boundary. *Deep Sea Research Part I: Oceanographic Research Papers*, 40(3), 561-582.  
827

828 Hellmer, H. H., Huhn, O., Gomis, D., & Timmermann, R. (2011). On the freshening of  
829 the northwestern Weddell Sea continental shelf. *Ocean Science*, 7(3), 305-316.  
830

831 Hellmer, H. H., Rhein, M., Heinemann, G., Abalichin, J., Abouchami, W., Baars, O., ...  
832 & Frank, M. (2016). Meteorology and oceanography of the Atlantic sector of the Southern  
833 Ocean—a review of German achievements from the last decade. *Ocean Dynamics*,  
834 66(11), 1379-1413.  
835

836 Heywood, K. J., Naveira Garabato, A. C., & Stevens, D. P. (2002). High mixing rates in  
837 the abyssal Southern Ocean. *Nature*, 415(6875), 1011-1014.

838  
839 Heywood, K. J., Schmidtko, S., Heuzé, C., Kaiser, J., Jickells, T. D., Queste, B. Y., ... &  
840 Guihen, D. (2014). Ocean processes at the Antarctic continental slope. *Philosophical*  
841 *Transactions of the Royal Society of London A: Mathematical, Physical and Engineering*  
842 *Sciences*, 372(2019), 20130047.

843  
844 Huhn, O., Hellmer, H. H., Rhein, M., Rodehacke, C., Roether, W., Schodlok, M. P., &  
845 Schröder, M. (2008). Evidence of deep-and bottom-water formation in the western  
846 Weddell Sea. *Deep Sea Research Part II: Topical Studies in Oceanography*, 55(8), 1098-  
847 1116.

848  
849 Ivanov, V. V., Shapiro, G. I., Huthnance, J. M., Aleynik, D. L., & Golovin, P. N. (2004).  
850 Cascades of dense water around the world ocean. *Progress in oceanography*, 60(1), 47-  
851 98.

852  
853 Jackett, D. R., & McDougall, T. J. (1997). A neutral density variable for the world's  
854 oceans. *Journal of Physical Oceanography*, 27(2), 237-263.

855  
856 Jacobs, S. S. (2004). Bottom water production and its links with the thermohaline  
857 circulation. *Antarctic Science*, 16(04), 427-437.

858  
859 Jenkins, W. J., Smethie, W. M., Boyle, E. A., & Cutter, G. A. (2015). Water mass analysis  
860 for the US GEOTRACES (GA03) North Atlantic sections. *Deep Sea Research Part II:*  
861 *Topical Studies in Oceanography*, 116, 6-20.

862  
863 Johnson, G. C. (2008). Quantifying Antarctic bottom water and North Atlantic deep water  
864 volumes. *Journal of Geophysical Research: Oceans*, 113(C5).

865  
866 Johnson, D. R., Garcia, H. E., & Boyer, T. P. (2013). *World Ocean Database 2013*  
867 *Tutorial*.

868  
869 Jullion, L., Jones, S. C., Naveira Garabato, A. C., & Meredith, M. P. (2010). Wind-  
870 controlled export of Antarctic Bottom Water from the Weddell Sea. *Geophysical*  
871 *Research Letters*, 37(9).

872  
873 Jullion, L., Naveira Garabato, A. C., Bacon, S., Meredith, M. P., Brown, P. J., Torres-  
874 Valdés, S., ... & Hoppema, M. (2014). The contribution of the Weddell Gyre to the lower  
875 limb of the Global Overturning Circulation. *Journal of Geophysical Research: Oceans*,  
876 119(6), 3357-3377.

877  
878 Jullion, L., Naveira Garabato, A. C., Meredith, M. P., Holland, P. R., Courtois, P., &  
879 King, B. A. (2013). Decadal freshening of the Antarctic Bottom Water exported from the  
880 Weddell Sea. *Journal of Climate*, 26(20), 8111-8125.

881  
882 Karstensen, J., & Tomczak, M. (1997). Ventilation processes and water mass ages in the  
883 thermocline of the southeast Indian Ocean. *Geophysical Research Letters*, 24(22), 2777-  
884 2780.

885  
886 Karstensen, J., & Tomczak, M. (1998). Age determination of mixed water masses using  
887 CFC and oxygen data. *Journal of Geophysical Research: Oceans*, 103(C9), 18599-18609.

888  
889 Karstensen, J., & Tomczak, M. (1999). Manual for OMP Analysis Package for  
890 MATLAB, version 2.0.  
891 Kerr, R., Mata, M. M., & Garcia, C. A. (2009a). On the temporal variability of the  
892 Weddell Sea Deep Water masses. *Antarctic Science*, 21(4), 383.  
893  
894 Kerr, R., Wainer, I., & Mata, M. M. (2009b). Representation of the Weddell Sea deep  
895 water masses in the ocean component of the NCAR-CCSM model. *Antarctic Science*,  
896 21(03), 301-312.  
897  
898 Kerr, R., K. J. Heywood, M. M. Mata, and C. A. E. Garcia (2012a), On the outflow of  
899 dense water from the Weddell and Ross Seas in OCCAM model, *Ocean Sci.*, 8(3), 369–  
900 388, doi:10.5194/os-8-369-2012.  
901  
902 Kerr, R., Wainer, I. L. A. N. A., Mata, M. M., & Garcia, C. A. (2012b). Quantifying  
903 Antarctic deep waters in SODA reanalysis product. *Pesquisa Antártica Brasileira*, 5, 47-  
904 59.  
905  
906 Kitade, Y., Shimada, K., Tamura, T., Williams, G. D., Aoki, S., Fukamachi, Y., ... &  
907 Ohshima, K. I. (2014). Antarctic bottom water production from the Vincennes Bay  
908 polynya, East Antarctica. *Geophysical Research Letters*, 41(10), 3528-3534.  
909  
910 Klatt, O., Fahrbach, E., Hoppema, M., & Rohardt, G. (2005). The transport of the Weddell  
911 Gyre across the Prime Meridian. *Deep Sea Research Part II: Topical Studies in*  
912 *Oceanography*, 52(3), 513-528.  
913  
914 Leach, H., Strass, V., & Cisewski, B. (2011). Modification by lateral mixing of the Warm  
915 Deep Water entering the Weddell Sea in the Maud Rise region. *Ocean Dynamics*, 61(1),  
916 51-68.  
917  
918 Leffanue, H., & Tomczak, M. (2004). Using OMP analysis to observe temporal  
919 variability in water mass distribution. *Journal of Marine Systems*, 48(1), 3-14.  
920  
921 Mackas, D. L., Denman, K. L., & Bennett, A. F. (1987). Least squares multiple tracer  
922 analysis of water mass composition. *Journal of Geophysical Research: Oceans*, 92(C3),  
923 2907-2918.  
924  
925 Mamayev, O.I., 1975. *Temperature-Salinity Analysis of World Ocean Waters*. Elsevier,  
926 Amsterdam.  
927  
928 Meredith, M. P. (2016). Understanding the structure of changes in the Southern Ocean  
929 eddy field. *Geophysical Research Letters*, 43(11), 5829-5832.  
930  
931 Meredith, M. P., Gordon, A. L., Naveira Garabato, A. C., Abrahamsen, E. P., Huber, B.  
932 A., Jullion, L., & Venables, H. J. (2011). Synchronous intensification and warming of  
933 Antarctic Bottom Water outflow from the Weddell Gyre. *Geophysical Research Letters*,  
934 38(3).  
935

936 Meredith, M. P., Heywood, K. J., Frew, R. D., & Dennis, P. F. (1999). Formation and  
937 circulation of the water masses between the southern Indian Ocean and Antarctica:  
938 Results from 18O. *Journal of marine research*, 57(3), 449-470.  
939

940 Meredith, M. P., Jullion, L., Brown, P. J., Garabato, A. C. N., & Couldrey, M. P. (2014).  
941 Dense waters of the Weddell and Scotia Seas: recent changes in properties and  
942 circulation. *Philosophical Transactions of the Royal Society of London A: Mathematical,*  
943 *Physical and Engineering Sciences*, 372(2019), 20130041.  
944

945 Meredith, M. P., Locarnini, R. A., Van Scoy, K. A., Watson, A. J., Heywood, K. J., &  
946 King, B. A. (2000). On the sources of Weddell Gyre Antarctic bottom water. *Journal of*  
947 *Geophysical Research: Oceans*, 105(C1), 1093-1104.  
948

949 Meredith, M. P., Mazloff, M., Sallée, J. B., Newman, L., Wahlin, A., Williams, M. J. M.,  
950 ... & Schmidtko, S. (2015). The Southern Ocean Observing System (SOOS). *Bulletin of*  
951 *the American Meteorological Society*, 96(7), S157-S160.  
952

953 Meredith, M. P., Naveira Garabato, A. C. N., Gordon, A. L., & Johnson, G. C. (2008).  
954 Evolution of the deep and bottom waters of the Scotia Sea, Southern Ocean, during 1995–  
955 2005. *Journal of Climate*, 21(13), 3327-3343.  
956

957 Meredith, M. P., Schofield, O., Newman, L., Urban, E., & Sparrow, M. (2013). The vision  
958 for a Southern Ocean observing system. *Current Opinion in Environmental Sustainability*,  
959 5(3), 306-313.  
960

961 Muench, R.D.; Hellmer, H. H. (2002). The international DOVETAIL program. *Deep Sea*  
962 *Research Part II: Topical Studies in Oceanography*  
963

964 Naveira Garabato, A. C., McDonagh, E. L., Stevens, D. P., Heywood, K. J., & Sanders,  
965 R. J. (2002). On the export of Antarctic bottom water from the Weddell Sea. *Deep Sea*  
966 *Research Part II: Topical Studies in Oceanography*, 49(21), 4715-4742.  
967

968 Naveira Garabato, A. C., Williams, A. P., & Bacon, S. (2014). The three-dimensional  
969 overturning circulation of the Southern Ocean during the WOCE era. *Progress in*  
970 *Oceanography*, 120, 41-78.  
971

972 Nicholls, K. W., Østerhus, S., Makinson, K., & Johnson, M. R. (2001). Oceanographic  
973 conditions south of Berkner Island, beneath Filchner-Ronne Ice Shelf, Antarctica. *Journal*  
974 *of Geophysical Research: Oceans*, 106(C6), 11481-11492.  
975

976 Foldvik, A., Gammelsrød, T., Østerhus, S., Fahrbach, E., Rohardt, G., Schröder, M., ... &  
977 Woodgate, R. A. (2004). Ice shelf water overflow and bottom water formation in the  
978 southern Weddell Sea. *Journal of Geophysical Research: Oceans*, 109(C2).  
979

980 Nicholls, K. W., Østerhus, S., Makinson, K., Gammelsrød, T., & Fahrbach, E. (2009).  
981 Ice-ocean processes over the continental shelf of the southern Weddell Sea, Antarctica:  
982 A review. *Reviews of Geophysics*, 47(3).  
983

984 Orsi, A. H., Jacobs, S. S., Gordon, A. L., & Visbeck, M. (2001). Cooling and ventilating  
985 the abyssal ocean. *Geophysical Research Letters*, 28(15), 2923-2926.

986  
987 Orsi, A. H., Johnson, G. C., & Bullister, J. L. (1999). Circulation, mixing, and production  
988 of Antarctic Bottom Water. *Progress in Oceanography*, 43(1), 55-109.  
989  
990 Orsi, A. H., Smethie, W. M., & Bullister, J. L. (2002). On the total input of Antarctic  
991 waters to the deep ocean: A preliminary estimate from chlorofluorocarbon measurements.  
992 *Journal of Geophysical Research: Oceans*, 107(C8).  
993  
994 Ohshima, K. I., Fukamachi, Y., Williams, G. D., Nihashi, S., Roquet, F., Kitade, Y., ... &  
995 Hindell, M. (2013). Antarctic Bottom Water production by intense sea-ice formation in  
996 the Cape Darnley polynya. *Nature Geoscience*, 6(3), 235-240.  
997  
998 Pardo, P. C., Pérez, F. F., Velo, A., & Gilcoto, M. (2012). Water masses distribution in  
999 the Southern Ocean: Improvement of an extended OMP (eOMP) analysis. *Progress in*  
1000 *Oceanography*, 103, 92-105.  
1001  
1002 Pritchard, H. D., & Vaughan, D. G. (2007). Widespread acceleration of tidewater glaciers  
1003 on the Antarctic Peninsula. *Journal of Geophysical Research: Earth Surface*, 112(F3).  
1004  
1005 Purkey, S. G., & Johnson, G. C. (2010). Warming of global abyssal and deep Southern  
1006 Ocean waters between the 1990s and 2000s: Contributions to global heat and sea level  
1007 rise budgets. *Journal of Climate*, 23(23), 6336-6351.  
1008  
1009 Purkey, S. G., & Johnson, G. C. (2012). Global contraction of Antarctic Bottom Water  
1010 between the 1980s and 2000s. *Journal of Climate*, 25(17), 5830-5844.  
1011  
1012 Purkey, S. G., & Johnson, G. C. (2013). Antarctic Bottom Water warming and freshening:  
1013 Contributions to sea level rise, ocean freshwater budgets, and global heat gain. *Journal of*  
1014 *Climate*, 26(16), 6105-6122.  
1015  
1016 Poole, R., & Tomczak, M. (1999). Optimum multiparameter analysis of the water mass  
1017 structure in the Atlantic Ocean thermocline. *Deep Sea Research Part I: Oceanographic*  
1018 *Research Papers*, 46(11), 1895-1921.  
1019  
1020 Rignot, E., Bamber, J. L., Van Den Broeke, M. R., Davis, C., Li, Y., Van De Berg, W. J.,  
1021 & Van Meijgaard, E. (2008). Recent Antarctic ice mass loss from radar interferometry  
1022 and regional climate modelling. *Nature Geoscience*, 1(2), 106-110.  
1023  
1024 Rintoul, S. R. (2007). Rapid freshening of Antarctic Bottom Water formed in the Indian  
1025 and Pacific oceans. *Geophysical Research Letters*, 34(6).  
1026  
1027 Rohardt, G., Fahrbach, E., and Wisotzki, A.: Physical oceanography during  
1028 POLARSTERN cruise ANT-XXVII/2, Alfred Wegener Institute, Helmholtz Center for  
1029 Polar and Marine Research, Bremerhaven, doi:10.1594/PANGAEA.772244, 2011.  
1030  
1031 Rohardt, Gerd; Boebel, Olaf (2015): Physical oceanography during POLARSTERN  
1032 cruise PS89 (ANT-XXX/2). Alfred Wegener Institute, Helmholtz Center for Polar and  
1033 Marine Research, Bremerhaven, doi:10.1594/PANGAEA.846701.  
1034



1035 Ryan, S., Schröder, M., Huhn, O., & Timmermann, R. (2016). On the warm inflow at the  
1036 eastern boundary of the Weddell Gyre. *Deep Sea Research Part I: Oceanographic*  
1037 *Research Papers*, 107, 70-81.  
1038

1039 Robertson, R., Visbeck, M., Gordon, A. L., & Fahrbach, E. (2002). Long-term  
1040 temperature trends in the deep waters of the Weddell Sea. *Deep Sea Research Part II:*  
1041 *Topical Studies in Oceanography*, 49(21), 4791-4806.  
1042

1043 Santos, G. C., Kerr, R., Azevedo, J. L. L., Mendes, C. R. B., & da Cunha, L. C. (2016).  
1044 Influence of Antarctic Intermediate Water on the deoxygenation of the Atlantic Ocean.  
1045 *Dynamics of Atmospheres and Oceans*, 76, 72-82.  
1046

1047 Schmidtko, S., Heywood, K. J., Thompson, A. F., & Aoki, S. (2014). Multidecadal  
1048 warming of Antarctic waters. *Science*, 346(6214), 1227-1231.  
1049

1050 Sloyan, B. M. (2005). Spatial variability of mixing in the Southern Ocean. *Geophysical*  
1051 *research letters*, 32(18).  
1052

1053 Sokolov, S., & Rintoul, S. R. (2009). Circumpolar structure and distribution of the  
1054 Antarctic Circumpolar Current fronts: 2. Variability and relationship to sea surface  
1055 height. *Journal of Geophysical Research: Oceans*, 114(C11).  
1056

1057 Schröder, M., & Fahrbach, E. (1999). On the structure and the transport of the eastern  
1058 Weddell Gyre. *Deep Sea Research Part II: Topical Studies in Oceanography*, 46(1), 501-  
1059 527.  
1060

1061 Schröder, M., Hellmer, H. H., & Absy, J. M. (2002). On the near-bottom variability in  
1062 the northwestern Weddell Sea. *Deep Sea Research Part II: Topical Studies in*  
1063 *Oceanography*, 49(21), 4767-4790.  
1064

1065 Talley, L. D. (2013). Closure of the global overturning circulation through the Indian,  
1066 Pacific, and Southern Oceans: Schematics and transports. *Oceanography*, 26(1), 80-97.  
1067

1068 Tomczak, M. (1981). A multi-parameter extension of temperature/salinity diagram  
1069 techniques for the analysis of non-isopycnal mixing. *Progress in Oceanography*, 10(3),  
1070 147-171.  
1071

1072 Tomczak, M. (1999). Some historical, theoretical and applied aspects of quantitative  
1073 water mass analysis. *Journal of Marine Research*, 57(2), 275-303.  
1074

1075 Tomczak, M., & Large, D. G. (1989). Optimum multiparameter analysis of mixing in the  
1076 thermocline of the eastern Indian Ocean. *Journal of Geophysical Research: Oceans*,  
1077 94(C11), 16141-16149.  
1078

1079 Tomczak, M., & Liefvink, S. (2005). Interannual variations of water mass volumes in the  
1080 Southern Ocean. *Journal of Atmospheric & Ocean Science*, 10(1), 31-42.  
1081

1082 van Caspel, M., Schröder, M., Huhn, O., & Hellmer, H. H. (2015). Precursors of Antarctic  
1083 Bottom Water formed on the continental shelf off Larsen Ice Shelf. *Deep Sea Research*  
1084 *Part I: Oceanographic Research Papers*, 99, 1-9.

1085  
1086 van Heuven, S. M., Hoppema, M., Huhn, O., Slagter, H. A., & de Baar, H. J. (2011).  
1087 Direct observation of increasing CO<sub>2</sub> in the Weddell Gyre along the Prime Meridian  
1088 during 1973–2008. *Deep Sea Research Part II: Topical Studies in Oceanography*, 58(25),  
1089 2613-2635.  
1090  
1091 van Heuven, S. M., Hoppema, M., Jones, E. M., & de Baar, H. J. (2014). Rapid invasion  
1092 of anthropogenic CO<sub>2</sub> into the deep circulation of the Weddell Gyre. *Phil. Trans. R. Soc.*  
1093 *A*, 372(2019), 20130056.  
1094  
1095 van Sebille, E., Spence, P., Mazloff, M. R., England, M. H., Rintoul, S. R., & Saenko, O.  
1096 A. (2013). Abyssal connections of Antarctic Bottom Water in a Southern Ocean state  
1097 estimate. *Geophysical Research Letters*, 40(10), 2177-2182.  
1098  
1099 von Gyldenfeldt, A. B., Fahrbach, E., García, M. A., & Schröder, M. (2002). Flow  
1100 variability at the tip of the Antarctic Peninsula. *Deep Sea Research Part II: Topical Studies*  
1101 *in Oceanography*, 49(21), 4743-4766.  
1102  
1103 Whitworth, T., & Nowlin, W. D. (1987). Water masses and currents of the Southern  
1104 Ocean at the Greenwich Meridian. *Journal of Geophysical Research: Oceans*, 92(C6),  
1105 6462-6476.  
1106  
1107 Whitworth, T., III, A. H. Orsi, S.-J. Kim, and W. D. Nowlin Jr., 1998. Water masses and  
1108 mixing near the Antarctic Slope Front. *Ocean, Ice, and Atmosphere: Interactions at the*  
1109 *Antarctic Continental Margin*, S. S. Jacobs and R. F. Weiss, Eds., Antarctic Research  
1110 Series, Amer. Geophys. Union, 1–27.  
1111  
1112 Wijk, E. M., & Rintoul, S. R. (2014). Freshening drives contraction of Antarctic bottom  
1113 water in the Australian Antarctic Basin. *Geophysical Research Letters*, 41(5), 1657-1664.